

REPORT DOCUMENTAT

AFRL-SR-BL-TR-98-

Form Approved
OMB No. 0704-0188

Public reporting burden for this collection of information is estimated to a gathering and maintaining the data needed, and completing and reviewing collection of information, including suggestions for reducing this burden, Davis Highway, Suite 1204, Arlington, VA 22202-4302, and to the Office

actions, searching existing data sources, den estimate or any other aspect of this Operations and Reports, 1215 Jefferson -0188), Washington, DC 20503.

1. AGENCY USE ONLY (Leave blank)		2. REPORT DATE 18 June 1998		3. REPORT TYPE AND DATES COVERED Final Technical Report 01 May 94 to 30 Apr 98	
4. TITLE AND SUBTITLE Fracture and Failure at and Near Interfaces Under Pressure				5. FUNDING NUMBERS F49620-94-1-0253	
6. AUTHOR(S) W. G. Knauss, PI					
7. PERFORMING ORGANIZATION NAME(S) AND ADDRESS(ES) Graduate Aeronautical Laboratories California Institute of Technology Pasadena, CA 91125				8. PERFORMING ORGANIZATION REPORT NUMBER	
9. SPONSORING/MONITORING AGENCY NAME(S) AND ADDRESS(ES) AFOSR/NA 110 Duncan Avenue, Ste B115 Bolling AFB, DC 20332-8050				10. SPONSORING/MONITORING AGENCY REPORT NUMBER F49620-94-1-0253	
11. SUPPLEMENTARY NOTES					
12a. DISTRIBUTION AVAILABILITY STATEMENT Approved for public release; distribution unlimited.					
13. ABSTRACT (Maximum 200 words) This work addressed the failure behavior of solid propellant rocket fuels through crack propagation. The objective of the study was to 1) develop the means for measuring large deformation fields around the tips of stationary or slowly moving cracks, to develop realistic data for comparison with improved analytical results, and to 2) initiate a new computational approach for stress analysis of cracks at and near interfaces, which can draw on the expanding capabilities of parallel processing. Important results are that 1) strain inhomogeneities are much more pronounced than hitherto anticipated; they are associated with the granular microstructure and are characterized by spatial variations on the sub-millimeter size scale; 2) these strain inhomogeneities dominate the deformation field around a crack tip and control the fracture process; cracks connect statistically distributed regions of high strain, if they are reasonably close to the crack propagation line; 3) a domain of 1-3 mm in extent around the crack tip is totally dominated by this highly inhomogeneously deformed material, with the adjacent material undergoing large nonlinear deformations; 4) the disintegrating region close to the crack tip is not likely to be describable in continuum terms, and needs to be modeled in a discrete fashion.					
14. SUBJECT TERMS				15. NUMBER OF PAGES	
				16. PRICE CODE	
17. SECURITY CLASSIFICATION OF REPORT Unclassified		18. SECURITY CLASSIFICATION OF THIS PAGE Unclassified		19. SECURITY CLASSIFICATION OF ABSTRACT Unclassified	
				20. LIMITATION OF ABSTRACT UL	

24 JUN 1993

Final Technical Report
to the
Airforce Office of Scientific Research
on Grant No. F49620-94-1-0253

**Fracture and Failure at and Near
Interfaces Under Pressure**

W. G. Knauss, PI

June 1998

**Graduate Aeronautical Laboratories
California Institute of Technology
Pasadena, California 91125**

Fracture and Failure at and Near Interfaces Under Pressure

Abstract

A research study is summarized that addressed the failure behavior of solid propellant rocket fuels through crack propagation. The objective of the study was to

- 1) develop the means for measuring large deformation fields around the tips of stationary or slowly moving cracks, in order to develop realistic data against which improved analytical results can be compared, and to
- 2) initiate a new computational approach for stress analysis of cracks in solid propellants at and near interfaces, which analysis can draw on the ever expanding capabilities of computationally parallel processing.

Correspondingly, both experimental and analytical/numerical work was carried out:

(A) Experimental work:

- (1) A full field method for visualizing and measuring deformation around the crack tip in a fracture process with large strains has been developed;
- (2) The method was applied to the fracture in a solid propellant (growth of a crack). It was found that large variations of strain occur in nominally "homogeneous" deformation fields, with strain variations by as much as factors of three.

(B) Computational/Analytical work:

- (1) Proposed and implemented a discrete-continuum approach to analyze damage evolution in solid propellant (particle-filled elastomers in general).
- (2) Established analytical stability conditions for interfacial dewetting at planar, cylindrical and spherical interfaces for uniform decohesion.
- (3) Applied the method to investigate the effect of particle interaction on the damage evolution in solid propellant: Small changes in particle geometry and spacing have large effects on particle debonding. Reattachments observed as part of the global dewetting process.

An important result of this study is that

- 1) strain inhomogeneities are much more pronounced than hitherto anticipated; they are associated with the granular microstructure of the material and are characterized by spatial variations on the sub-millimeter size scale;
- 2) these strain inhomogeneities dominate the deformation field around a crack tip and control the fracture process, in that cracks tend to connect statistically distributed regions of high strain, if they are reasonably close to the crack propagation line;
- 3) a domain of 1-3 mm in extent around the crack tip is totally dominated by this highly inhomogeneously deformed material, with the adjacent material undergoing large nonlinear deformations;
- 4) the disintegrating region close to the crack tip is not likely to be describable in continuum terms, and needs to be modeled in a discrete fashion.

1. Introduction

Since the development of solid propellant rocket motors in the late 1950', an important operational and design consideration has always been the reliable functioning and readiness of both tactical and strategic missile systems. The most important and most difficult component of the system analysis has been the predictability or suppression of failure by the initiation and/or propagation of cracks in the fuel charge or grain. Such failures typically arise in the grain at "star points" or at the support interface of the grain to the motor case. Either situation is equally detrimental, because crack initiation can lead to propagation as a result of the highly transient pressure pulse during ignition, or during long term storage while awaiting deployment. For tactical missiles the exposure to under-wing use during readiness maneuvers provides an additional deleterious use environment.

Two aspects of fracture analysis and prediction in composite propellants have concerned the mechanics community ever since the start of solid propellant use, and for neither has a satisfactory solution been found in the roughly four intervening decades: One addresses the experimental determination of the strain fields around the tips of cracks in these materials; the other is the computation of stress fields either from these strains or from other "first" principles. Virtually all analyses have been based on variants of linearly elastic analyses, which have long been known to provide estimates at best, since the nonlinear characteristics of the propellant materials have been well established for several decades. However, the means of dealing with that type of material characterization is not at all well in hand nor has it been developed for applications to motor design.

1.1 A new way for stress analysis involving high strain (stress) gradients.

For over three decades propellant stress analysis has been accomplished by means of finite element codes that started with linearly elastic material characterization. While specialty codes have been developed, to address nonlinear behavior of the material, they have neither been demonstrated in connection with appropriate experimental input, nor are the constitutive equations used for them particularly germane to propellants. All these computations have to be supplemented with a heavy dose of empiricism based on years of practical experience to make failure estimation roughly comparable with motor performance.

The most common assumption underlying these analyses is that, in spite of its microstructure, the propellant is an essentially homogeneous material. The consequence of this assumption is that strain fields are smoothly varying and maxima — drivers of failure initiation — occur where continuum theory says they should occur. We shall see that the experimental analysis of this question tells us otherwise, and the variations in strain fields arising from inhomogeneities is indeed very significant. The consequence for failure prediction is then that such behavior needs to be incorporated into analyses. The question of how to do this is not answered simply.

Typically propellants have been modeled as (homogeneous) continua. That approximation seems reasonable when the strain variations are not important in the fracture sense and when the domain considered is large in comparison to the domains in which inhomogeneities dominate. However, when these latter domain sizes are on the order of domains that determine fracture, such as at the front of a crack, then continuum representations are no longer appropriate. Attempts have been made over the past years to characterize the disintegrating material at the crack tip as a continuum with highly nonlinear properties. Thus the odd situation arises whereby one discretizes the crack tip domain, tries to find a "smeared-out" or average continuum model of the failing material, and then derives from that a failure criterion that comes close to the physical situation that is truly discrete in its failure aspects.

Nonlinear behavior is widely observed in particulate composites, such as solid propellants, tires, toughened plastics, even when global deformations are relatively small. Global nonlinearity in particulate composites is often caused by cavitation or tear (appearance of voids in the matrix) and/or by interfacial particle debonding or "dewetting"; see Schippel(1920), Smith(1959), Farris(1964), Oberth (1967), Knauss and Mueller (1979) and Gent and Park (1984). Dewetting and interfacial void generation occurs when the bond at an interface is relatively weak; otherwise cavitation can occur. How to represent this damaged-material behavior in continuum terms for finite element analyses has been a long standing question. Constitutive models containing damage have been proposed, for example, by Farris and Schapery (1973), Schapery (1986), Govindjee and Simo (1992), Vratsanos and Farris (1993) and Ravichandran and Liu (1995). However, these models, excepting that Govindjee and Simo (1992), are typically restricted to infinitesimal elastic/viscoelastic matrix behavior, and therefore their applications in regions of high deformation gradients such as a crack tip, are, at best, questionable. More importantly, one must critically examine the implied proposition of first representing a truly

discontinuous process by a homogenized continuum formulation and then turn around and formulate a new local failure criterion that addresses the crack propagation process by means of the homogenized material description in such a way that the true physical process of the discrete micro crack growth and coalescence is reproduced faithfully near the crack tip.

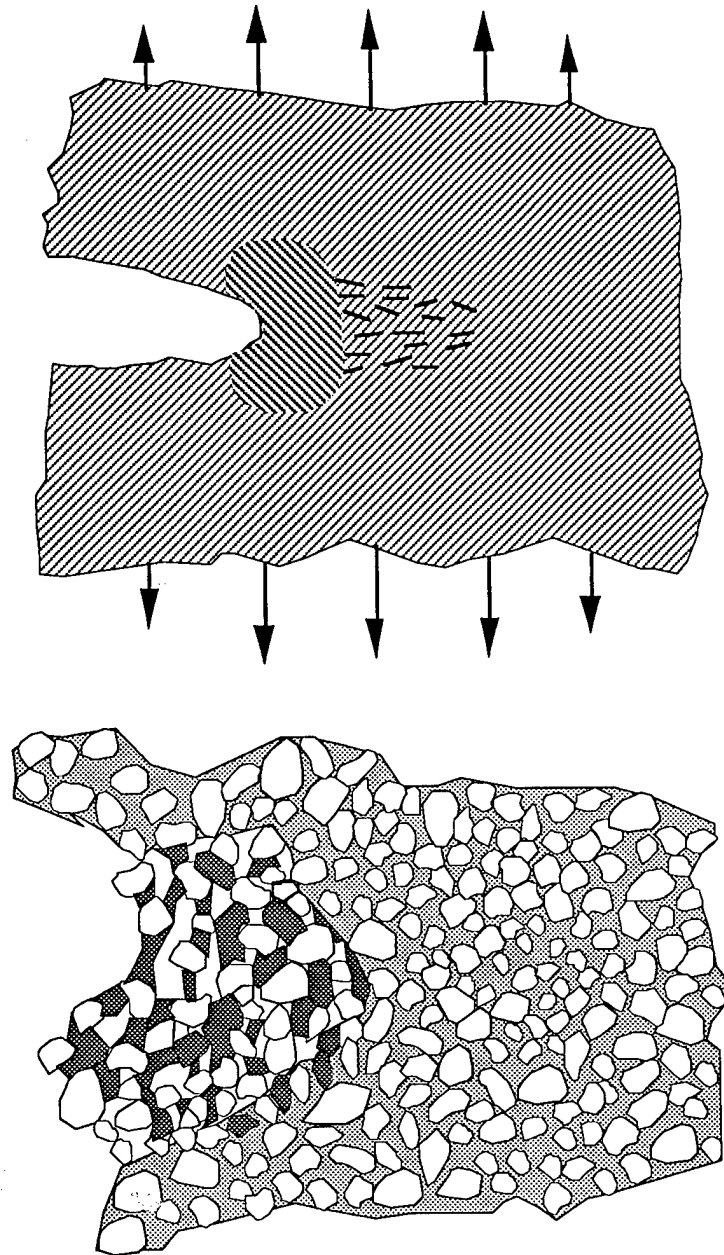


Figure 1: Above: Tripartition of the crack tip domain, with local discrete behavior at the crack tip, nonlinear continuum response farther away, and linear behavior over the rest of the large solid. Below: Detailed account of the crack tip region close to the crack tip. Dark areas represent voids, gray areas binder and white particles.

An alternate way to crack tip characterization, that circumvents this circuitous route for computing involving two approximation schemes is, thus, to treat the zone around the crack tip in a discrete fashion, that is, ultimately with statistical particle distributions, and deal with the failure around individual particles.

It appears, therefore, more reasonable to characterize the material locally near a crack tip in a discrete manner by modeling a select region of the high strain gradient domain through discretely failing elements embedded in another and larger region of nonlinear and/or linear material response. Here failure sites ultimately become the fracture sites by which a crack propagates through void coalescence. Such a hybrid discrete-continuum approach appears feasible in light of the ever more rapidly increasing power of computing machines. We thus pursue here initially the time-independent (non-viscoelastic) problem of the dewetting process allowing for large deformation in the matrix material, and with the intention of incorporating the results into a larger finite element analysis for crack growth studies in particulate composites.

Figure 1 shows such an approach graphically: A small zone around the crack tip is modeled with individual particles, the next farther (but "close in") domain from the crack tip as a continuum possessing nonlinear characteristics, and the remainder of the structure is sufficiently well characterized by linear behavior since the strains tend to be rather small there.

1.2. Experimental definition of the discrete analysis domain

Experimental observations are necessary to assess the size of the domain within which discretization of particulate mechanics is appropriate. This endeavor was the first part of the project and revolved around microscope studies of deformations and strain determination through the Digital Image Correlation Method (DIC). In this we concentrated on the microdamage evolution and its interaction with small cracks. One observes clearly that the deformation in solid propellants is inhomogeneous at the length scale of particles (especially in high deformation regions, e.g. near a crack tip), while the deformation is "homogeneous" at a larger length scale. Experimental observations indicate that

microdamage-induced heterogeneity plays the dominant role in crack propagation and the strain distribution field near a crack tip.

The Digital Image Correlation Method.

Because the modifications to the original Digital Image Correlation code (DIC) sought here are closely tied to the inner workings of the algorithm for the two-dimensional correlation scheme, the latter is summarized briefly. A three-dimensional extension to the code is presented in "Submicron Deformation Field Measurements Part II: Improved Digital Image Correlation" by Vendroux, G. and Knauss, W.G., *Experimental Mechanics*, 38, No. 2, pp. 86-92, June 1998.

Two-dimensional Digital Image Correlation

A surface profile, as obtained, for example, by a Scanning Tunneling Microscope, is a discrete record of the "height" of the surface at grid points assigned to a specimen surface. Let $f(x,y)$ represent the surface profile of a specimen in an undeformed state at point $G(x,y)$, and $g(\tilde{x}, \tilde{y})$ the surface profile after deformation at the corresponding point $\tilde{G}(\tilde{x}, \tilde{y})$. If the profile pattern before deformation is uniquely related to the profile pattern after deformation, a correlation of these two patterns exists to detect the profile difference which represents the object deformation. Let χ be the mapping from the undeformed to the deformed configuration

$$G \rightarrow \tilde{G} = \chi(G) \quad \text{such that} \quad g(\tilde{x}, \tilde{y}) = f(x,y) \quad (1)$$

or

$$\begin{aligned} \tilde{x} &= x + u(x,y) \\ \tilde{y} &= y + v(x,y) \end{aligned} \quad (2)$$

with u and v the in-plane displacements of G , and let $\tilde{G}_0(\tilde{x}_0, \tilde{y}_0)$ be the image of $G_0(x_0, y_0)$ through χ ; further, let S be a (sub)set of points around G_0 and \tilde{S} the corresponding (sub)set of point around \tilde{G}_0 . Assuming that S is sufficiently small, eq (2) can be expanded into

$$\tilde{x} = x + u(x_0, y_0) + \frac{\partial u}{\partial x} \Big|_{x_0, y_0} (x - x_0) + \frac{\partial u}{\partial y} \Big|_{x_0, y_0} (y - y_0) \quad (3a)$$

$$\tilde{y} = y + v(x_0, y_0) + \frac{\partial v}{\partial x} \Big|_{x_0, y_0} (x - x_0) + \frac{\partial v}{\partial y} \Big|_{x_0, y_0} (y - y_0) \quad (3b)$$

as the linearization χ_l of χ around G_0 . For a discrete set of data define the correlation coefficients

$$C = \frac{\sum_{G_s \in S} [f(G_s) - g(\chi_l(G_s))]^2}{\sum_{G_s \in S} f^2(G_s)} \quad (4a)$$

or

$$C = 1 - \frac{\sum_{G_s \in S} f(G_s)g(\chi_l(G_s))}{[\sum_{G_s \in S} f^2(G_s) \sum_{G_s \in S} g^2(\chi_l(G_s))]^{\frac{1}{2}}} \quad (4b)$$

It is clear that C will be zero when the coefficients of the mapping $\chi_l \{ \dots \}$ are indeed the displacements and their derivatives at G_0 [4, 8]. The best estimate of these values are determined by minimizing C, which process can be viewed as a non-linear optimization scheme, some details of which will be discussed in section 3.2 under "Optimization Scheme".

2. Analytical

The numerical work has centered on developing segment or elements containing particles, which undergo the dewetting process. The issues for resolution were primarily the stability of the dewetting process in the computational model. We believe that this problem is now well in hand. In a similar vain, the stability of cracks branching from the dewetting void to fracture the binder is similarly handled. As a result of this research it has also become clear that a somewhat coarser modeling of the dewetting/fracture process is tolerable. It is, by now, abundantly clear that the proposed scheme of highly detailed particle induced failure around crack tips can be treated numerically with the currently available (parallel) computing systems. Moreover, problems smaller than full-scale motor applications can be addresses probably without parallel processing. This assessment is based on our experience that less refined damage models around particles can now be constructed.

3. Report content

In the following development the experimental work is presented first. That presentation is followed by a delineation of the numerical modeling. However, because these studies have been already documented in written reports and publications they are only abstracted and summarized here, with the full papers denoted by an asterisk '*' attached as appendices.

3.1. Strain Inhomogeneity and Discontinuous Crack Growth in a Particulate Composite.

This topic has been documented as an Aeronautical Engineer's Thesis under the title:

Gonzales, J.;

Full Field study of Strain Distribution near the Crack Tip in the Fracture of Solid Propellants via Large Strain Digital Image correlation and Optical Microscopy; Engineer's Thesis, 1996, California Institute of Technology, Pasadena, CA 91125

Abstract

A full field method for visualizing deformation around the crack tip in a fracture process with large strains is developed. A digital image correlation program (DIC) is used to incrementally compute strains and displacements between two consecutive images of a deformation process. Values of strain and displacements for consecutive deformations are added, this way solving convergence problems in the DIC algorithm when large deformations are investigated. The method developed is used to investigate the strain distribution within 1 mm of the crack tip in a particulate composite solid (propellant) using microscopic visualization of the deformation process.

A paper based on that work will appear in September 1998 in the *International Journal of Solids and Structures*:

Gonzales, J. and Knauss, W.G.;

Strain Inhomogeneity and Discontinuous Crack Growth in a Particulate Composite*;

Abstract

A full field method for visualizing deformation around the crack tip in a fracture process with large strains is developed. Digital Image Correlation (DIC) is used to incrementally compute strain and displacements between consecutive images in a global deformation process. Values of strains and displacements for consecutive deformations are added, this

way solving convergence problems in DIC algorithm when large deformation are investigated. The method developed here is used to investigate the strain distribution within 1mm of the crack tip in a particulate composite solid propellant. It is shown that in "nominally" homogeneous deformations (unidirectional deformation of a propellant sheet) the strains vary over a range of a factor of three, with the average corresponding to the global strain defined as the ration of boundary displacement and the specimen width or height. In crack propagation studies such high strain regions are the loci for crack propagation.

A second presentation of essentially the same material entitled

Strain Distribution around Cracks in Damaged Particle-Filled Elastomers has been made by J. Gonzales at the 1997 Composite Conference held at Hawaii in July 1997.

The standard use of the Digital Image Correlation (DIC) works well to investigate deformations where the maximum principal strain is less than 10%. For studying deformation when this limit is reached, it is necessary to use additional tools like the Large Deformation Digital Image Correlation (LD-DIC). This method performs well using the standard DIC in a stepwise manner, following the deformation history. Results for two tests on a particle-filled elastomer are presented using the LD-DIC. The strain associated with void-opening in a particle-filled elastomer (solid propellant) is addressed in the first test while the effect of damage on the strain distribution in a crack opening problem for the same material is investigated in the second situation.

3.2. The next papers cover the numerical/analytical work on the deformation of damage mechanics in particulate filled composites.

This phase of the research addresses the micromechanics of a dewetting particulate composite to model both the failure progression as well as the global force-displacement (stress-strain) response. The idea is that such a model becomes the small-scale "finite element" for a larger propellant domain in which damage and failure progress as coupled to the nonlinear response of the local material.

The first paper is

Zhong, X.A. and Knauss, W.G.

Analysis of Interfacial Failure in Particle-Filled Elastomers*

Journal of Engineering Materials and Technology (ASME Transactions); **119**, pp. 198-204, July 1997 (presented at the 1997 ASME/ASCE/SES Joint Summer Meeting at Northwestern University, McNu'97)

Abstract

The evolution of microdamage (interfacial dewetting) in highly filled elastomers under consideration of high deformation gradients is examined with the aid of the ABAQUS code in a two dimensional setting. The interface between hard (rigid, two dimensional) inclusions embedded in an elastomer characterized by a three-term (rate insensitive) Ogden model, is represented by a cohesive-zone type interfacial model to follow the whole process of interfacial dewetting and its effect on the global (multiphase) material response in plane strain. The analysis is carried out through a mixed finite element formulation for hyperelasticity, incorporating interface elements. We consider the effects of particle geometry and loading conditions on the process of interfacial failure. The results indicate that the distributed failure process is highly unstable and depends heavily on the size, shape, orientation and interactions of inclusions as well as the global loading conditions. The overall material behavior of the model agrees qualitatively with experimental observation this instability discovery has prompted the investigation considered.

Zhong, X.A. and Knauss, W.G;

On the Stability of Phase Separation in a Finite Solid with Interfaces*;

Accepted for publication in *Mechanics of Composite Materials and Structures*.

Abstract

The stability of homogeneous phase separation in finite solids containing planar, cylindrical or spherical interfaces is investigated analytically. Explicit stability conditions are deduced for each interface geometry. It is shown how the interaction of load (force or displacement) material properties of the phases and interface properties jointly determine the stability of the interface separation process.

Zhong, X.A. and Knauss, W.G;
Effects of Particle Interaction and Size Variation on Damage Evolution in Filled Elastomers*
Submitted to "Mechanics of Materials".

Abstract

A micromechanical analysis of damage evolution (interfacial debonding) in particulate filled elastomers addresses the effect of the interactions between particles and of the variation in filler size. The composite is treated as an assembly of two constituents in a finite element model. The interaction between particles controls the damage evolution: (1) For high volume fractions, a relatively small change in particle size has a surprisingly large effect on the local material response, (2) for large differences in particle sizes (*e.g.* bimodal distribution), damage occurs at interfaces between large particles and the matrix, with limited damage occurring at the small particles. While these effects of particle interaction and size variation are smoothed out in a large ensemble of particles, it is foreseeable that they are an important factor in a failure process such as macroscopic crack propagation, which spans scales considerably larger than the maximum particle size. Specifically, one expects thus that in the vicinity of a macroscopic crack the large particles become the sites for small cracks which coalesce to larger ones and join up with the macro crack, while the small particles operate primarily so as to locally stiffen the matrix without incurring significant damage in their vicinity.

4. Archival Publications

1. Gonzales, J.; **Full Field study of Strain Distribution near the Crack Tip in the Fracture of Solid Propellants via Large Strain Digital Image correlation and Optical Microscopy**; Engineer's Thesis, 1996, California Institute of Technology, Pasadena, CA 91125
2. Gonzales, J. and Knauss, W.G.; **Strain Inhomogeneity and Discontinuous Crack Growth in a Particulate Composite**; *Journal of the Physics and Mechanics of Solids*; to appear September 1998.
3. Zhong, X.A. and Knauss, W.G.; **Analysis of Interfacial Failure in Particle-Filled Elastomers**; *Journal of Engineering Materials and Technology* (ASME Transactions); vol 119, pp. 198-204, July 1997
4. Zhong, X.A. and Knauss, W.G.; **On the Stability of Phase Separation in a Finite Solid with Interfaces**; Accepted for publication in *Mechanics of Composite Materials and Structures*.
5. Zhong, X.A. and Knauss, W.G.; **Effects of Particle Interaction and Size Variation on Damage Evolution in Filled Elastomers**; Submitted to "Mechanics of Materials".

5. Interaction and Dissemination of Results

1. "A Program of Failure/Fracture Analysis Relevant to Interfacial Fracture in Solid Rocket Motors", presented at the JANNAF Propulsion Sub-Committee Joint Meeting, Tampa, FL, December 4-8, 1995.
2. "Time Dependence of Decohesion", presented at the International Conference on Adhesion at Huazhong University, Wuhan, Hubei, PRC, China, November 1-4, 1995.
3. "Changes in the Experimentalist's Role in the Future of Mechanics", (W.G. Knauss) presented at the IMM Think Tank on the Role of Experiments in the Mechanics and Physics of Solids and Structures, University of Houston, Houston, TX, March 24-26, 1996.
4. "Viscoelastic Material Characterization and Fracture", (W.G. Knauss) presented at IMM's Mechanics-Materials Linkage 1996 Summer School, University of California at San Diego, San Diego, CA, July 22-August 2, 1996.
5. "A New Computational Model for Stress Analysis of Solid Propellant Rocket Fuel", (W.G. Knauss) presented at the JANNAF Propulsion Conference, Albuquerque, NM, December 9-13, 1996.
6. "Strain Inhomogeneity and Discontinuous Crack Growth in a Particulate Composite", (with Javier Gonzalez), presented at the Rodney J. Clifton Symposium, California Institute of Technology, Pasadena, CA, May 1997.
7. "Analysis of Interfacial Failure in Particle-Filled Elastomers", (with A. Zhong), presented at McNu 1997, Northwestern University, Evanston, IL, June 29-July 2, 1997.
8. "Diagnostic Technologies in Experimental Mechanics", (W.G. Knauss) presented at the Fifth Summer School of the IMM's "Mechanics-Materials Linkage", The Catholic University of America, Washington, D.C., August 4-15, 1997.
9. "The Stability of a Finite Solid Containing Interfaces with Reference to Failure of Filled Elastomer", (with A. Zhong), presented at McNu 1997, Northwestern University, Evanston, IL, June 29-July 2, 1997.
10. "Strain Distribution Around Cracks in Damaged Particle-Filled Elastomers" (J. Gonzales) Composite Conference, Hawaii, July 1997.
11. "Analysis of Interfacial Failure in Particle-Filled Elastomers", (with A. Zhong), presented at McNu 1997, Northwestern University, Evanston, IL, June 29-July 2, 1997.
12. "High Resolution Measurement in Solid Mechanics", (W.G. Knauss) presented at the Institute of Physics Conference, "Modern Practice in Stress and Vibration Analysis", University College Dublin, Dublin, Ireland, September 3-5, 1997.
13. "Computational Mechanics and the Response of Particulate Composites", (with A. Zhong), presented at the Elastomer-FEA Forum '98, University of Akron, Akron, OH, March 19-20, 1998.

STRAIN INHOMOGENEITY AND DISCONTINUOUS CRACK GROWTH IN A PARTICULATE COMPOSITE

JAVIER GONZALEZ and W. G. KNAUSS

Graduate Aeronautical Laboratories, California Institute of Technology, Pasadena,
CA 91125, U.S.A.

ABSTRACT

A full field method for visualizing strain fields around a crack tip under large strains is developed. Digital image correlation is used to compute strains and displacements incrementally between consecutive images in a process of large deformations. Values of strain and displacements for these consecutive deformations are added such that convergence of the DIC algorithm is assured. The method is used to investigate the strain distribution in a globally homogeneously strained particulate composite (solid propellant) as well as in a zone close to (~ 2 mm) the crack tip in such a material by using a microscope. It is found that maximal strain variations deviate by as much as a factor of three from the average strain; additionally, observations on the interaction of strain inhomogeneities with the tip of a macroscopic crack are discussed.

Keywords: A. fracture, A. strain localization, B. inhomogeneous material, B. viscoelastic material, C. digital image correlation.

1. INTRODUCTION

Particulate composites are widely used in engineering. In the automotive industry, for example, carbon black filled rubbers are used in tires. Many injection molded materials are filled with small particles, while other rigid polymers are toughened through the addition of rubber particles. Solid propellant rocket fuels are physical mixtures of mostly ammonium perchlorate and aluminum powder, often in a multimodal size distribution, bonded together by a rubber phase called the matrix. Failure in all these materials is heavily dependent upon the interaction between the particles and the matrix, specifically on the separation of particles and binder. Failure also depends on the volume ratio of particles to matrix, which is typically close to 75% in solid propellant materials, but only in the range of 15 to 40% in structural polymers. In the sequel we examine the failure progression in a solid propellant (Triokol TPH 1011). Application of continuum mechanics to the stress/strain analysis of structures made of these types of materials typically invoke macroscopically homogeneous material performance, even though deformations are anything but homogeneous at the size scale of the particles. We shall see that inhomogeneous deformations occur at a size scale that is significantly larger than the largest particle, and that the failure process is directly related to the micro-structural deformations associated with these inhomogeneities.

Measuring large strains over small domains of tens to hundreds of microns is not a trivial matter. Imprinted grids tend to serve well at a size scale just above what is required here. Determining the micromechanical deformation with the aid of optical microscopy, *e.g.* at the tip of a macroscopic crack, implies the need to extend the presently available tools of strain measurements. In principle the digital image correlation method [Sutton *et al.*, 1983, 1985, 1986 and 1989], [Vendroux / Knauss, 1994] is ideal for this purpose except that it is not suitable if the deformations are so large that convergence of the correlation algorithm is no longer guaranteed: We shall see that deformations involving strains much in excess of 10% cause convergence failure of the DIC algorithm. On the other hand, strains on the order of 50% to 100% are typical for crack propagation problems in the materials of interest here. Accordingly we develop an

incremental application of the DIC method that is capable of analyzing large deformation histories. This development is first addressed in section 2, and followed, in section 3, by a discussion of the experimental setup for two sets of experiments: The first experiment addresses, in section 4, locally inhomogeneous deformations in a globally homogeneous deformation field, and the second examines the deformation field around the tips of a (slowly growing) crack in section 5, with particular interest centering on the inhomogeneity of the material response in the immediate crack tip region. The paper is summarized with concluding remarks in section 6.

2. DIGITAL IMAGE CORRELATION

Developed by Sutton and his colleagues [1983, 1985, 1986 and 1989] and improved by Vendroux and Knauss [1994], the digital image correlation (DIC) program is used to measure the displacement field and its gradients from images of an undeformed and deformed body. These are gray level images consisting of a grid of pixels, (typically 640 by 480) with eight-bit gray levels (0 to 255 levels). In the sequel we discuss problems arising with large deformations and a remedy to the situation through a step-wise method we call Large Deformation Digital Image Correlation (LD-DIC).

2. 1. Effect of Strain Level in Code Convergence

The problem in applying the DIC program to compute strain distributions in a large deformation process is, essentially, the failure of the DIC algorithm to converge from an initial solution estimate. The reasons for non-convergence may be diverse. The two major ones are changes of shadows from a fixed light source coupled with large motions of the surface, and, in the present case, possibly an inhomogeneous evolution of the deformation images. If one considers that the (rate of) convergence depends on the closeness of an initial estimate for the result (see the study on the radius of convergence by Vendroux and Knauss (1997) it becomes reasonable that failure can occur at even

moderate strains. Clearly, more definitive rules for code failure or success depend on the specific experimental conditions.

To assess the effect of the strain level on the convergence of the DIC code, consider a test on a homogeneous silicone rubber sheet stretched uniaxially, for which the resultant undeformed and deformed images associated with stretches from 0% to 40% are compared with the aid of DIC. For each deformation the strains and displacements were computed at 300 points. The fraction of points at which the numerics for the correlation optimization converged is presented in Figure 1 as a function of the Lagrangian strain.

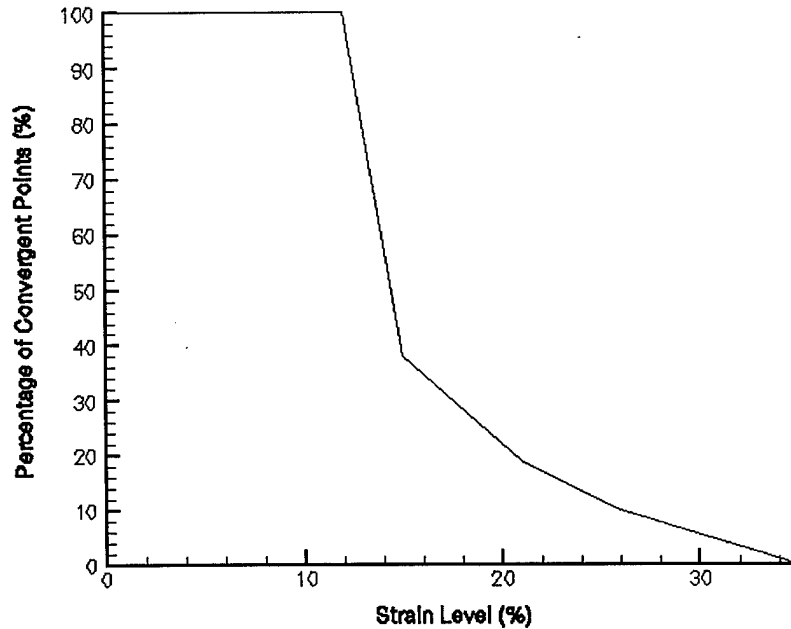


Figure 1. Successful convergence of the DIC algorithm as a function of (Lagrangian) strain level.

It is apparent that for deformations in excess of 10% a pronounced decrease occurs in the number of points with successful convergence. For the purpose of studying cracked solid propellants, where typically strains in excess of 30% need to be measured, the applicability of the standard DIC method is thus seriously compromised and a new or extended analysis tool is required.

2. 1. The Large Deformation Digital Image Correlation Method

To illustrate a proposed Large Deformation Digital Image Correlation (LD-DIC), consider a sequential deformation process on a body: Initially undeformed, the body undergoes a continuous deformation, called the “global deformation”. Consider three configurations of the body at three different instants during this global deformation. The first configuration describes the undeformed state of the body and the second a deformed state under a set of changed surface (and body) forces. Call this first segment of the global deformation “deformation A”. Next, an increment in the surface and body forces deforms the body further, this next incremental deformation being designated by “B”. The state of the body after deformation B is represented by the third configuration. Each configuration corresponds to an experimentally determined and temporally ordered set of images, say, the 1st, 2nd and 3rd. We select load parameters such that, by assumption, the DIC code can converge successfully to the proper increments of displacements and displacement gradients for the two separate deformations. However, the strains between configurations 1 and 3 (global deformation) are presumed larger than those that cause convergence failure. The LD-DIC method computes the deformation for the third state from the deformations in the two separate steps. To this end compute the global deformation gradient tensor $\mathbf{F}_{\text{global}}$ as the product of the individual deformation gradients

$$\mathbf{F}_{\text{global}} = \mathbf{F}_B \mathbf{F}_A \quad (1)$$

The DIC program determines the displacements of deformation A and their gradients for a discrete set of points G_i defined on a rectangular grid with respect to the first (reference) configuration. For demonstration purposes, these points are represented in configuration 1 in Figure 2 as a coarse rectangular grid. At the end of deformation A, material particles of the body at the grid points have moved to the points \tilde{G}_i in configuration 2 as signified by the non-orthogonal grid. By comparing the position of the points G_i and \tilde{G}_i in configurations 1 and 2 the DIC program yields the displacements u^A_i

and v^A_i , and the associated gradients $u^A_{x_i}$, $v^A_{y_i}$, $u^A_{y_i}$ and $v^A_{x_i}$ where the index “i” signifies the individual initial positions of the G_i .

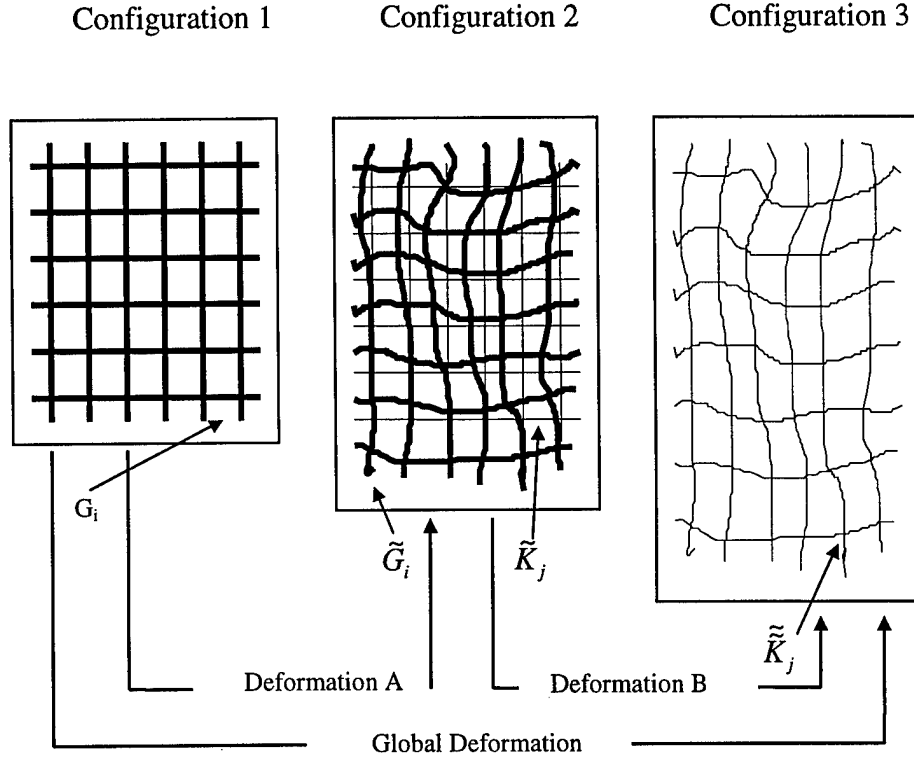


Figure 2. The interpolation process.

The displacements and displacements gradients are computed in a Lagrangian reference frame the coordinates of which are $\mathbf{X} = \{X_{1i}, X_{2i}\}$. Upon denoting the displacement components as u^A_i the motions of the material points are then represented by

$$\tilde{G}_i(\mathbf{X}_i) = G_i(\mathbf{X}_i) + \mathbf{u}^A_i(\mathbf{X}_i) \quad , \quad (2)$$

During the second deformation (B), the displacements and their gradients are computed for a different set of material particles which are located in configuration 2 at

the grid points \tilde{K}_j of an orthogonal grid, shown in Figure 2 as the fine grid. In deformation B these points are mapped onto the set $\tilde{\tilde{K}}_j$ in configuration 3. $\tilde{\tilde{K}}_j$ is again represented in the Lagrangian reference frame $\mathbf{Y}_i = \{Y_{1i}, Y_{2i}\}$ of configuration 2 as

$$\tilde{\tilde{K}}_j(\mathbf{Y}_i) = \tilde{K}_j(\mathbf{Y}_i) + \mathbf{u}_j^B(\mathbf{Y}_i) \quad (3)$$

To obtain the global deformation (A+B) it is necessary to assure that the material points of the first deformation are the same as for the second one. It is thus necessary to interpolate the results from the DIC for deformation B onto the locations of the material particles or grid points of the first (reference) configuration to obtain the displacements and their gradients $u^B_i, v^B_i, u_x^B_i, v_y^B_i, u_y^B_i$ and $v_x^B_i$ relative to configuration 1. The interpolation at the coordinates \tilde{G}_i is achieved by constructing a set of piecewise continuous surfaces from bilinear patches (plane surfaces). These are determined from the coordinates \tilde{K}_j of configuration 2 so that the displacements and displacement gradients of the initial set of material points are now known.

Using the subscript “gl” to denote global variables, one finds the global displacement components as

$$\begin{aligned} \mathbf{u}_{gl} &= \mathbf{u}^A + \mathbf{u}^B \\ \mathbf{v}_{gl} &= \mathbf{v}^A + \mathbf{v}^B. \end{aligned} \quad (4)$$

and their gradients are, upon invoking the tensorial relation (1),

$$\begin{aligned} [u_x]_{gl} &= u_x^A + u_x^B + u_x^A u_x^B + u_y^B v_x^A \\ [v_y]_{gl} &= v_y^A + v_y^B + v_y^A v_y^B + v_x^B u_y^A \\ [u_y]_{gl} &= u_y^A + u_y^B + u_y^A u_x^B + u_y^B v_y^A \\ [v_x]_{gl} &= v_x^A + v_x^B + u_x^A v_x^B + v_y^B v_x^A \end{aligned} \quad (5)$$

From which the (global) two-dimensional Lagrangian strain tensor derives, by definition, as

$$\begin{aligned}
 2E_{xx} &= 2[u_x]_{gl} + \{[u_x]_{gl}^2 + [v_x]_{gl}^2\} \\
 2E_{yy} &= 2[v_y]_{gl} + \{[u_y]_{gl}^2 + [v_y]_{gl}^2\} \\
 2E_{xy} &= \{[u_y]_{gl} + [v_x]_{gl}\} + \{[u_x]_{gl}[u_y]_{gl} + [v_x]_{gl}[v_y]_{gl}\}
 \end{aligned} \tag{6}$$

Here the displacement gradients of the displacement “w” normal to the surface have been neglected. This is permissible (even) for this situation of “plane stress” since under these large deformations the propellant material voids considerably so that the effective Poisson ratio is rather small, thus giving rise to only small gradients. For a global deformation requiring more than two steps the same is applied consecutively such that the second-to-the last increment is treated like the first one in the two-step example outlined here.

When more than two steps are needed for field evaluations there arises a loss of information at the boundary. This is the result of interpolating information near and internal to the boundary. As more and more steps are required the information near the boundary becomes increasingly corrupted due to the interpolation process and thus information is lost there. This loss is evident in the field images presented later on as apparent white-out regions along a boundary, including the flanks of a crack. Minimization of this feature still requires future attention.

2. 3. Verification of the Scheme for Addition of Fields

In order to check the efficacy of the proposed multi-step scheme we examine experimentally a specimen of homogeneous silicone rubber without a crack and coated with microscopic speckles, stretched sequentially and uniaxially to a maximum (Lagrangian) strain of 0.70 in a sequence of 12 deformation steps of 3-4% strain each (13

images). These strains were recorded (optically) with the aid of a microscope by keeping track of special markers (\equiv prescribed strain). Also, by using the information generated by the DIC program for every sub-deformation and the Large Deformation DIC method, the strains corresponding to images 1 and 2, images 1 and 3, *etc.*, were computed, up to the deformation of image 15 relative to image 1.

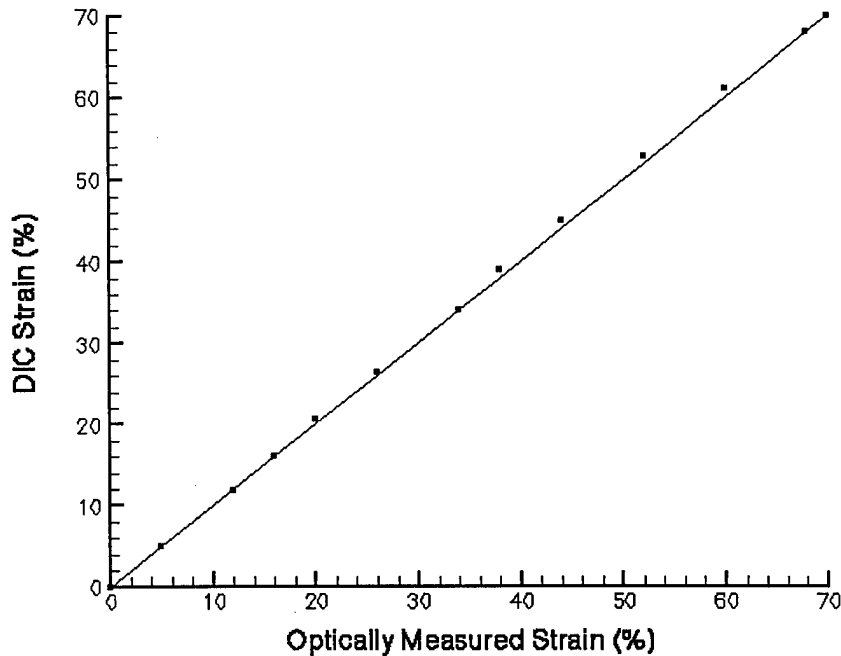


Figure 3. Comparison of strains determined optically and by the LD-DIC method; the solid line is the ideal relation.

Figure 3 shows the result as a comparison of the (optically) prescribed strain and the Large Deformation DIC computed (Lagrangian) strains. The maximum deviation occurs at a strain of 40%, amounting to only a 1% difference between the strain determined through the microscope and by the large deformation DIC method, a precision that is very acceptable for experimental mechanics investigations.

3. EXPERIMENTAL SETUP FOR DEFORMATION STUDIES

The equipment used for the experimental work on the particulate composite (solid propellant) has been described elsewhere in detail by Gonzalez, (1997). Includes a straining stage driven by a stepping motor through a flexible cable. The straining stage is, in turn, mounted on a positioning stage, for which a joy-stick controller allows the positioning of the straining stage under the objective of a Nikon microscope (Measurescope MM-22), a CCD camera and a personal computer with a frame grabber unit.

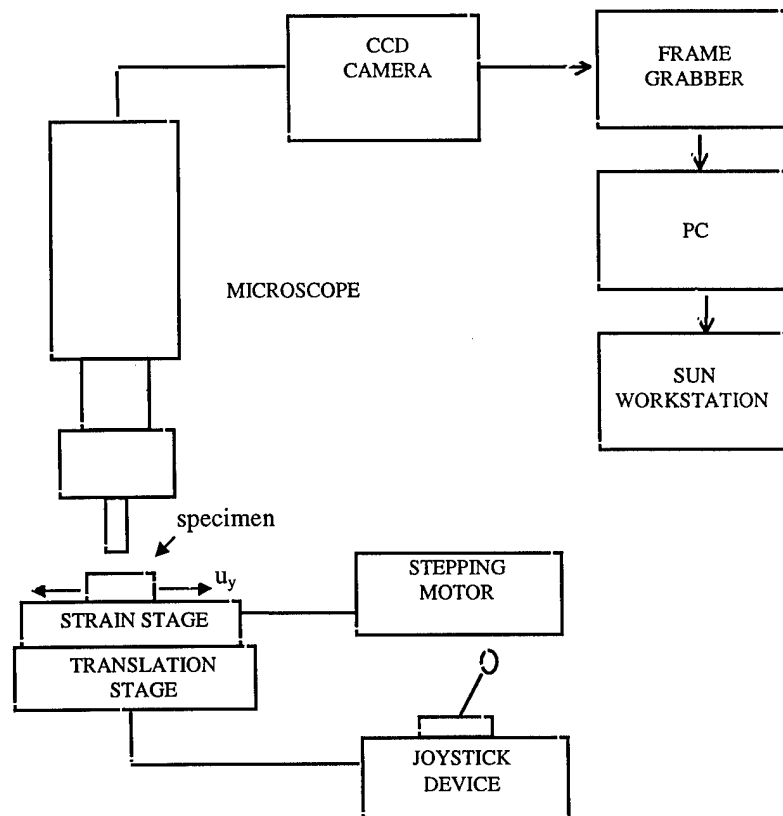


Figure 4. Schematic of the Experimental Setup

The images from the experiment are processed on a Sun workstation. A schematic of the experimental setup is shown in Figure 5.

4. LOCALLY INHOMOGENEOUS DEFORMATIONS IN A GLOBALLY HOMOGENEOUS DEFORMATION FIELD.

Before considering the problem of the strain distribution around the tip of a crack we examine the inhomogeneity of strains in a solid propellant sample subjected to uniform deformations at the specimen boundary (globally homogeneous deformation). To this end a sheet sample of propellant [5 cm x 2 cm x 0.3 cm] is strained uniformly in the direction parallel to the 2 cm dimension; after normalization by the 2 cm dimension that boundary displacement is called the “applied strain”. In Figure 5 we show a 2.5 mm x 2.55 mm field from the center region of the specimen as resolved through a microscope and deduced with the aid of the LD-DIC algorithm. The false color scheme clearly identifies the inhomogeneous character of the strain field, and from this map it is quite clear that the variations in the strain values are not only very significant, but that the “material properties” vary to a like degree in these regions.

It is of interest to dwell briefly on the scale of the inhomogeneous regions. While the latter are not sharply defined, it is, nevertheless, clear that these domains are measured in terms of millimeters and not microns. One might argue that a variation in properties in a small region (a hole or a hard, well-bonded particle) embedded in a homogeneous field renders deviation from that field several times larger than the defect itself. The reference problem of a circular hole in an elastic infinite sheet suggests that a noticeable perturbation in its vicinity is on the order of three times its diameter. While it is not our purpose to analyze in detail here the precise origin of every inhomogeneity, be it one of larger strain than the average or of a smaller value, it appears clear that these inhomogeneities are produced either by clusters of particles or by the presence or absence of individual ones.

To quantify the inhomogeneity of the strain field further, consider a plot of the strain along the line in Figure 5 as shown in Figure 6. The magnitude of these strains vary

by as much as a factor of three, although the average of the strain in Figure 6 represents closely the applied global strain of 1.5 %.

The distribution of these inhomogeneities defines a macroscopic size scale below which the assumption of homogeneous material properties is not justified. Stated alternately, in order to be able to assign homogeneous properties to such a composite it is necessary to deal with a size scale that is several times larger than the spacing between the regions of inhomogeneity. That region is, however, at least on the order of five mm or more.

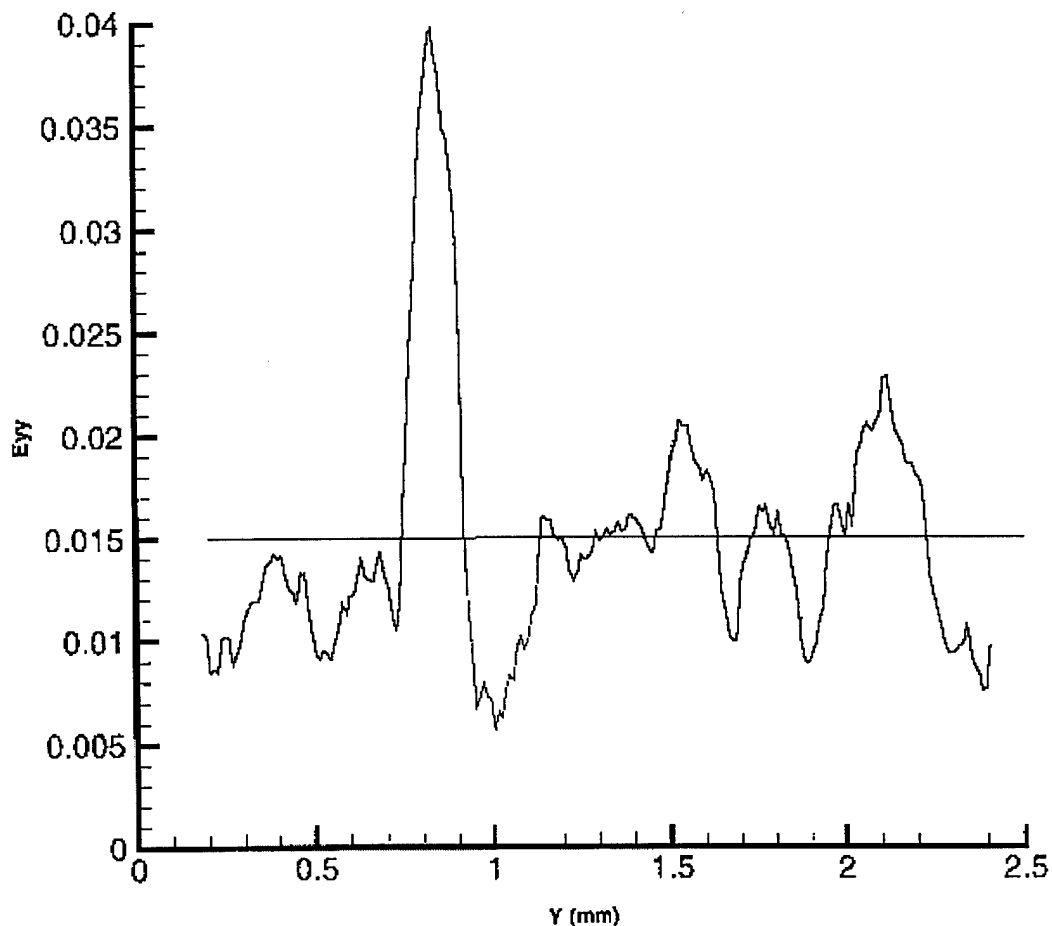


Figure 6. E_{yy} Distribution along the trace $x=1.4\text{mm}$ in Figure 5, parallel to the tension axis.

We shall see that this size scale is important in the analysis of the failure/fracture process considered next, since in this context this size limitation emphasizes the dependence of the fracture process on the statistical nature of the medium.

5. THE STRAIN FIELD NEAR THE TIP OF A CRACK

Having examined the distribution of strains in a globally homogeneous deformation field we turn next to examining the deformations in the close vicinity of a crack tip. We describe first the experimental set-up and then proceed to the analysis of the results.

5. 1. Experimental Aspects

A cracked specimen of solid propellant TPH 1011 is deformed globally at a constant strain rate 0.001 1/sec in the direction perpendicular to the crack. The crack, cut initially with a razor blade, opens commensurately. Its opening process is monitored through a microscope at 25x power. Five digital images of 640 x 480 pixels, representing 4 mm x 5 mm of the specimen surface were acquired every 10 seconds, corresponding to global (Lagrangian) strains of $E_{yy} = 0\%$, 1%, 2%, 3% and 4%.

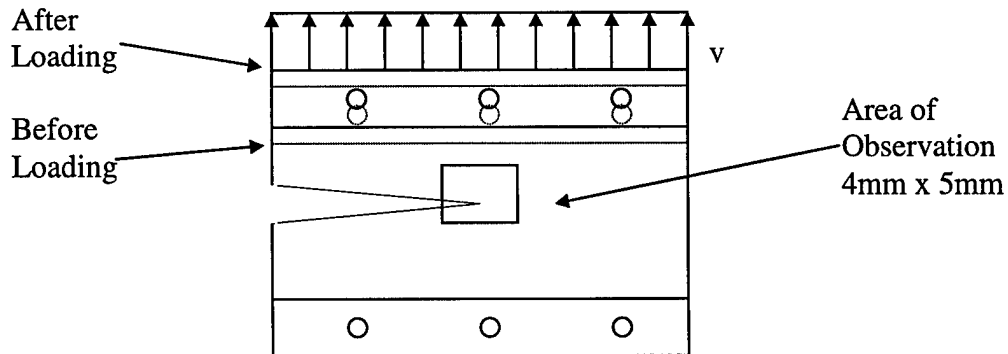


Figure 7. Specimen geometry and straining of a specimen.

The dotted lines represent the deformed geometry.

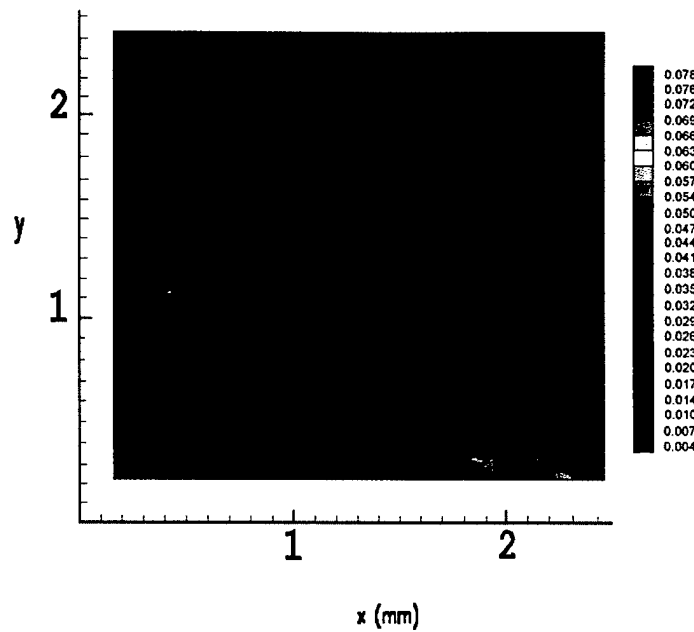


Figure 5: Inhomogeneous strain distribution in an integral specimen “homogeneously” deformed to 1.5% Global Strain¹.

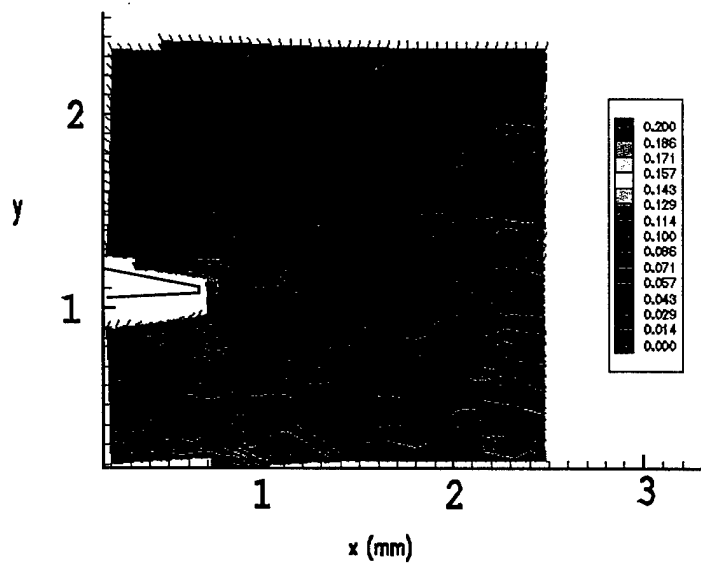


Figure 8: Maximum Principal Strain Distribution for 2% Global Strain.

¹ Note that the red domains surrounding the (green) high strain regions are the result of clustering of the red contour lines, not strain concentrations in themselves.

Although each of the images, excepting the first, is associated with different deformations we select here only two loads or deformation levels for illustrative purposes. Application of the (multi-step) LD-DIC code renders deformation maps as shown in figures 8 and 9.

Recall that because the multi-step method loses information at the boundary in each step the crack appears wide open and as having a very blunt tip. This appearance is the consequence of the multi-step method, so that Figures 8 and 9 do not represent the crack opening shape correctly; instead the shape has been sketched in as outlines.

5. 2. Results

We demonstrate results for the global strain of 2 and 4%. While deformations at higher load levels can be obtained, their interpretation is more troublesome since it involves (more) motion of the crack tip. As an example we present (false color) plots of the maximum principal strain at 2 % global deformation in Figure 8 and both the maximum and minimal principal strains for 4 % in Figures 9a and 9b. The two strain levels are presented primarily to afford a comparison for two progressively larger strains. By comparing Figures 8 and 9a one can readily see how the inhomogeneities develop early and essentially grow in intensity with the global strain. In passing from 2 to 4 % of global strain, a small amount of crack growth has taken place as is evident from comparing Figures 8 and 9a.

As before, the amplitude of the (Lagrangian) strain is represented by colors and contours and the small lines represent the orientation of the corresponding principal axes. Note that although the maximum principal axes should be basically parallel to the applied global displacement(s), at least in the region ahead of the crack tip, there are numerous locations where marked differences occur from this orientation. These differences are associated with the material strain inhomogeneities discussed in section 4. The same observation applies to the map of the minimum principal strain in Figure 9b for which the orientations

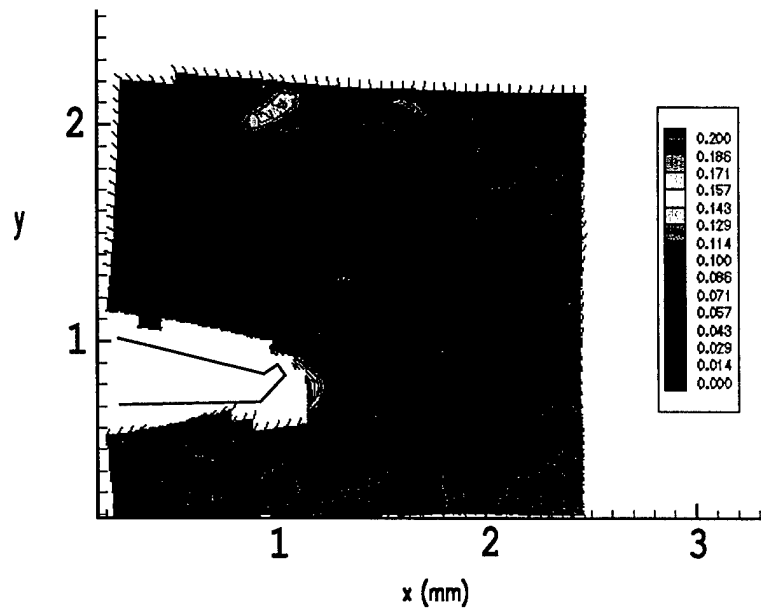
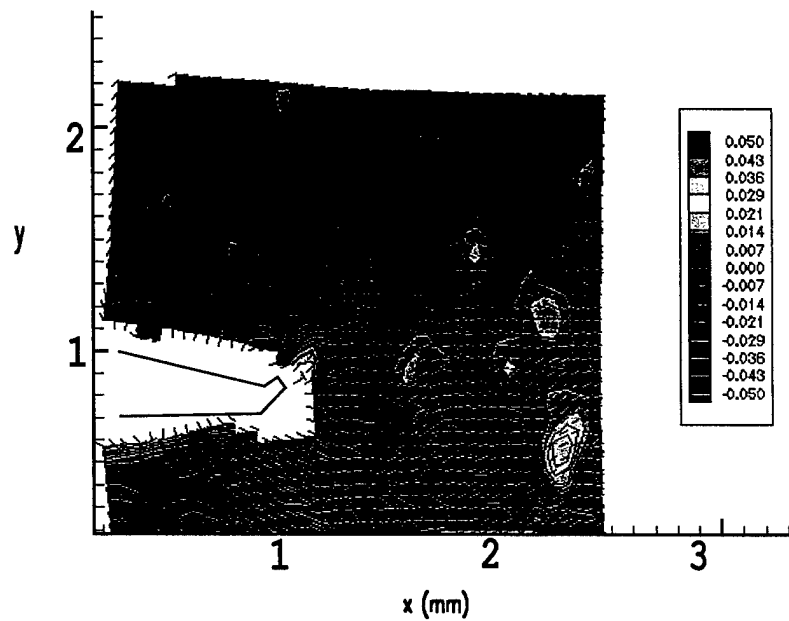


Figure 9. Principal Strain Distribution for a Far Field Strain of 4%

(a) Maximum Principal Strain (upper)

(b) Minimum Principal Strain (lower)



(small line segments) are generally orthogonal to those for the maximum principal strain. Also, compare the scale associated with the inhomogeneities and the distance of the high strain region relative to the crack tip. It is clear that the strain inhomogeneities cannot be separated from or submerged in the strain field of the crack tip: The crack tip strains are intimately connected with the scale of the material inhomogeneity. We note in particular that at this size of the viewing field the lobes that are part of the typical crack tip strain field for isotropic and homogeneous material are absent in the domain of observation or at most apparent in vestigial form; they are present only outside of the 2.5 mm x 2.5 mm observation area.

One feature of interest and identifiable in figures 8 and 9 is the localization of high strain within a roughly circular area of 0.5 mm radius around the crack tip. Figure 8, which shows the maximum principal strains and directions for 2% far field strain, shows deformation localization around the crack tip in two locations. One, partially visible, is centered on the current crack tip (at $x=0.7\text{mm}$, $y=1.1\text{mm}$) and about 150 microns in radius. The other concentration is centered on the position (0.7mm, 0.8mm), where it reaches a maximum principal strain of about 11%. However, that location does not become a part of the crack propagation process as is evident by its persistence in Figure 9a. Adjacent to these strain concentrations is a domain of about 5% local strain which includes the position (1.1mm, 1mm) where the orientation of the maximum principal strains is nearly aligned with the crack rather than being normal to it². At this position a void develops under subsequently increased deformation. This void is visible in Figure 10, which represents the image of the specimen for a 5% global deformation.

We have dwelled on these details to some extent in order to demonstrate that the observation of the surface of the failing material is not always indicative of how and where the crack is likely to propagate. Because one identifies strain inhomogeneities on the surface, it stands to reason that similar distributions exist through the thickness of the

² Similar situations prevail in Figure 7 at locations (1.6 mm, 0.9 mm), (2.1 mm, 1.1 mm) and (2.2 mm, 1.6 mm). In these regions the strains remain small, indicating that they are associated with rigid domains inside the specimen and under the surface.

specimen. Thus, the observations offered here point to a truly three-dimensional process. However, it is quite clear that the domain in which the failure process is prominently operative is confined to a domain on the order of half, but not more than one millimeter. This observation agrees with the results of Liu [Liu, C.T., 1997] who observed a similarly confinement of the process zone to a very small region. So much is clear from these studies, only portions of which are reported here, namely that crack propagation occurs by opening up voids which are typically high strain regions, distributed statistically throughout the material, and through joining of these voids with the main crack.

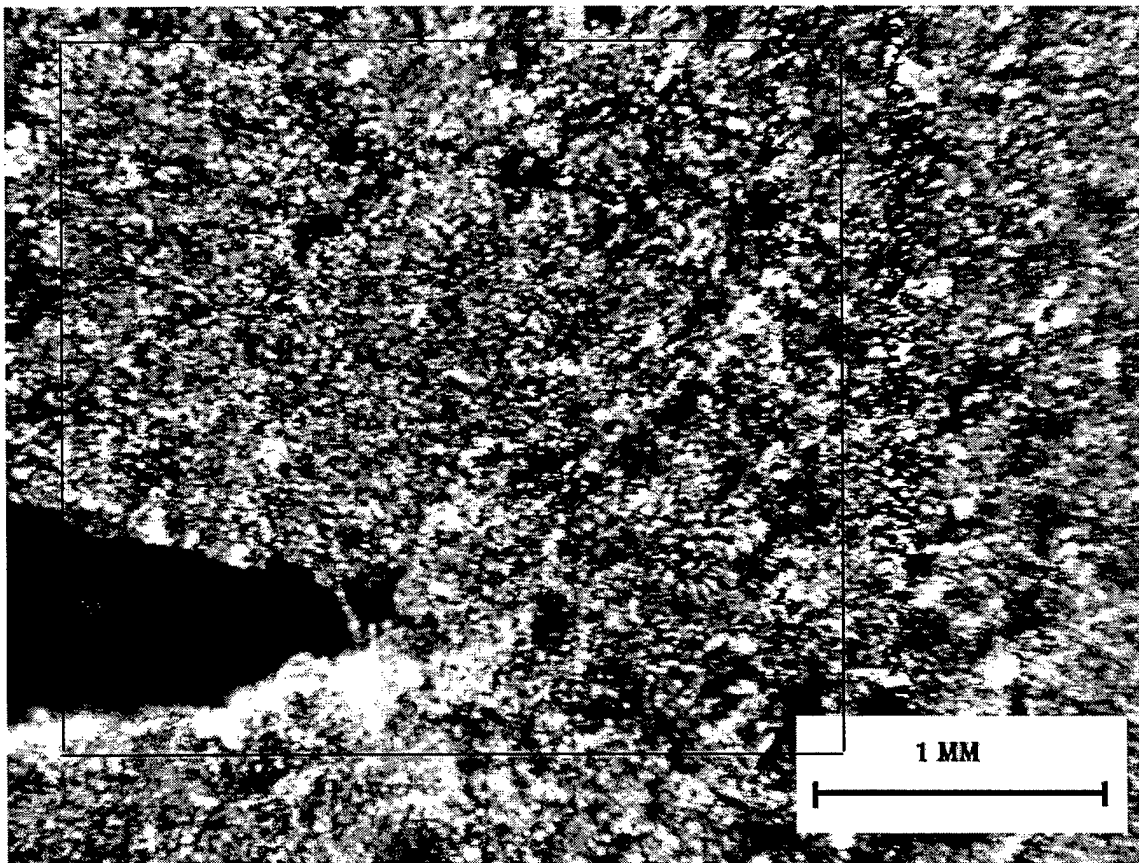


Figure 10. Micrograph of the crack tip region at a global strain of 5%. The “void” at the crack tip was a region of “small” ($\sim 5\%$) surface strain in Figure 8.

6. CONCLUDING REMARKS

The method of digital image correlation has been extended to large deformations by dividing the strain range into intervals within each of which DIC converges. The sequential extension renders satisfactory results with deviations not exceeding 1% from the prescribed strain field. This method has allowed resolution of highly inhomogeneous deformations embedded in a globally homogeneous deformation field. It is then demonstrated that this method can be applied to the analysis of strains around the tip of a crack in a particulate composite (solid propellant rocket fuel).

The, perhaps, most striking result of that investigation is the surprisingly large, inhomogeneous variations in the local strain field in a globally homogeneously deformed solid propellant material. It is apparent that the inherent heterogeneity of the material plays a key role for distribution of strains around the crack tip and its propagation. A second important observation is the fact that most of the deformation related to the crack propagation process localizes in a region around the crack tip of only about 0.5mm radius. Although there exist strain concentration domains outside of this small region on or close to the specimen surface, these deformations are insufficiently high to cause void formation of the strain concentrations so that they do not become sources of coalescence with the macroscopic crack. There is evidence, however, that the three dimensional distribution of strain inhomogeneities through the thickness of the specimen plays a role that mimics their in-plane distribution. There is no reason to suppose otherwise for this kind of particulate solid. Certainly some of the features visible on the surface are the consequence of single particles and particle agglomerations buried just beneath the surface.

Acknowledgements

This work was performed under grant AFOSR F49626-94-1-0253 from the Airforce Office of Scientific Research, with Dr. Walter F. Jones and Major Brian Sanders

as monitors. Also the frequent interaction with Dr. C. T. Liu of the Airforce Phillips Laboratory (Edwards Airforce Base) is gratefully acknowledged.

REFERENCES

- Bruck, H. A., McNeil, S. R., Sutton, M. A. and Peters, W. H. (1989) Digital Image Correlation using Newton-Raphson method of partial differential correlation. *Experimental Mechanics*, **29**. 261-267.
- Chu, T. C., Ranson, W. F., Sutton, M. A. and Peters, W. H. (1985) Applications of Digital Image Correlation techniques to experimental mechanics. *Experimental Mechanics*, **25**. 232-244.
- Farris, R. J. (1968) The Character of the Stress-Strain Function for Highly Filled Elastomers. *Trans. Soc. Rheol.*, **12**. 303-314.
- Farris, R. J. And Schapery, R. A. Development of a Solid Rocket Propellant Nonlinear Viscoelastic Constitutive Theory. Technical Report AFRPL-TR-73-50, Air Force Rocket Propulsion Laboratory, Edwards, CA.
- Gonzalez, J. (1997) Full Field Study of Strain Distribution Near the Crack Tip in Fracture of Solid Propellant Via Large Deformation Digital Image Correlation and Optical Microscopy. Aeronautical Engineer's Thesis, California Institute of Technology.
- Liu, C. T. (1991) Evaluation of Damage Fields Near Crack Tips in a Composite Solid Propellant. *Journal of Spacecrafts and Rockets*, **28**. 64-72.
- Liu, C. T. (1997) The Effect of Micro Damage on Time-Dependent Crack Growth in a Composite Solid Propellant. *Mech. Time-Dependent Materials*, **1**. 123-136.
- Ravichandran, G. and Liu, C. T. (1995) Modeling Constitutive Behavior of Particulate Composites Undergoing Damage. *Int. J. Solids Structures*, **32**. 979-990.
- Sutton, M. A., Walters, W. J., Peters, W. H., Ranson, W. F. and McNeil, S. R. (1983) Application of an optimized Digital Image Correlation method to planar deformation analysis. *Image Vision Computing*, **4**. 143-150.
- Sutton, M. A., Cheng, M., Peters, W. H., Chao, Y. J. and McNeill, S. R. (1986) Application of an Optimized Digital Correlation Method to Planar Deformation Analysis. *Experimental Mechanics*, **4**. 143-150.

- Vendroux, G. and Knauss, W. G. (1994) Submicron Deformation Field Measurements: II. Improved Digital Image Correlation. GALCIT SM Report 94-5. To appear in *Experimental Mechanics*.
- Vratsanos, L. and Farris, R. (1993) A Predictive Model for the Mechanical Behavior of Particulate Composites. Part II: Comparison of the Model Predictions to Literature Data. *Polymer Engineering and Science*, **33**. 1466-1474.
- Zhong, X. and Knauss, W. G. (1997) Analysis of Interfacial Failure in Particulate Filled Elastomers. Submitted to *ASME J. Eng. Materials and Tech.*

Analysis of Interfacial Failure in Particle-Filled Elastomers

X. Allan Zhong

Wolfgang G. Knauss

Graduate Aeronautical Laboratories,
California Institute of Technology,
Pasadena, CA 91125

The evolution of microdamage (interfacial dewetting) in highly filled elastomers under consideration of high deformation gradients is examined. The interface between hard (rigid, two-dimensional) inclusions embedded in an elastomer characterized by a three-term Ogden (rate insensitive) model, and the elastomer matrix is represented by a cohesive-zone type interfacial model to follow the whole process of interfacial dewetting and its effect on the global (multiphase) material response in a plane strain setting. The analysis is carried out through a mixed finite element formulation for hyperelasticity, incorporating interface elements. We consider the effects of particle geometry and loading conditions on the process of interfacial failure. The results indicate that the distributed failure process is highly unstable and depends heavily on the size, shape, orientation and interactions of inclusions as well as the global loading conditions. The overall material behavior of the model agrees qualitatively with experimental observation.

1 Introduction

Nonlinear behavior is widely observed in particulate composites, such as solid propellants, tires, toughened plastics, even when global deformations are relatively small. Global non-linearity in particulate composites is often caused by cavitation or tear (appearance of voids in the matrix) and/or by interfacial particle debonding or "dewetting"; see Schippel (1920), Smith (1959), Farris (1964), Oberth (1967), Knauss and Mueller (1979), and Gent and Park (1984). Dewetting and interfacial void generation occurs when the bond at an interface is relatively weak; otherwise cavitation can occur. How to represent this damaged-material behavior in continuum terms for finite element analyses has been a long standing question. Constitutive models containing damage have been proposed, for example, by Farris and Schapery (1973), Schapery (1986), Govindjee and Simo (1992), Vratsanos and Farris (1993), and Ravichandran and Liu (1995). However, these models (except Govindjee and Simo, 1992) are typically restricted to infinitesimal elastic/viscoelastic matrix behavior, and therefore their applications in a high deformation gradient area, such as a crack tip, are, at best, questionable. More importantly, one must critically examine the implied proposition of first representing a truly discontinuous process by a homogenized continuum formulation and then turn around and formulate a new local failure criterion that addresses the crack propagation process by means of the homogenized material description in such a way that the true physical process of the discrete micro crack growth and coalescence is reproduced faithfully near the crack tip.

By contrast, it appears more reasonable to characterize the material locally near a crack tip in a discrete way by modeling a select region of the high strain gradient domain through discretely failing elements embedded in another and larger region of nonlinear and/or linear material response as illustrated in Fig. 1. Such a hybrid discrete-continuum approach appears feasible in light of the ever more rapidly increasing power of computing machines. We thus pursue here initially the time-independent (nonviscoelastic) problem of the dewetting process allowing for large deformation in the matrix material, and with the intention of incorporating the results into a larger finite element analysis for crack growth studies in particulate composites.

In addition to interfacial debonding, we consider here the formation and growth of voids, as well as their interaction in (high) strain gradients. The aim is to apply these physical micro-phenomena to global failure in these types of composites: macroscopic regions of stress concentrations are to be represented by an assemblage of micro-mechanically detailed "superelements," their individual force transmissions and failure responses governing the failure procession of global composites. Thus our interest is not limited to unit-cell problems, but aims at much larger scale problems in order to address the failure/fracture process in particulate composites. Because the domain for this distinctly discrete process of failure has been shown to be very limited in extent (Liu, 1991; Gonzalez and Knauss, 1997) it may suffice to deal with a rather small number of "superelement," say on the order of 200 to 300.

To this end one needs to characterize the debonding of particles from the matrix material with the key issue being the characterization of the properties of a matrix-particle interface, including its failure response. This issue has been addressed repeatedly, for example, by Ungsuwarungsri and Knauss (1987), Needleman (1987, 1990), and Yeh (1992). Interfacial constitutive models are sometimes called cohesive-zone type models as they resemble the cohesive-zone model (Barenblatt, 1962; Dugdale, 1960) in fracture mechanics. There are basically two approaches to characterize an interface at the continuum level. One utilizes a nonlinear spring model to mimic the interfacial failure process; the other employs a potential for formulating an interfacial "constitutive relation." The common feature is that they relate interfacial tractions to relative displacements at interfaces. Here we employ a simple nonlinear foundation model which is similar to that of Ungsuwarungsri and Knauss (1987), the parameters of which can be ultimately determined by fitting numerical solution to corresponding experimental results. We implement the proposed interfacial constitutive relation through interface elements which have been widely used in computational contact problems, rock joints, concrete mechanics; see for example, Beer (1985), Zubelewicz and Bazant (1987), and Schellekens and De Borst (1993).

Though an elastomer is a time-dependent viscoelastic material, we consider the elastomer, for simplicity reasons, to be characterized by a hyperelastic Ogden material (Ogden, 1972). Because the elastomer matrix is soft compared to the particles, we consider the latter to be rigid.¹ In order to gain insight into

¹Contributed by the Materials Division for publication in the JOURNAL OF ENGINEERING MATERIALS AND TECHNOLOGY. Manuscript received by the Materials Division January 2, 1997; revised manuscript received April 14, 1997. Associate Technical Editor: Ellen M. Arruda.

¹This choice is made for convenience. Under high rate loading, the binder may be stiff by compression so that the particles will also deform. That case is computationally treatable as well, but requires larger computational resources.

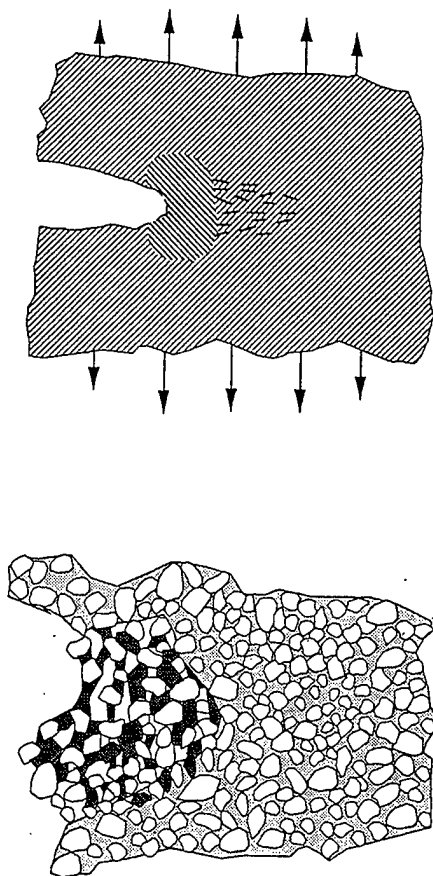


Fig. 1 A discretely failing region embedded in a linear/nonlinear material

this approach and to test numerical strategies, a two dimensional version of the problem is considered first. Furthermore the bond at interfaces is assumed to be "weak" so that only interfacial debonding needs to be considered (no cavitation in the elastomer). A three-dimensional problem description is left to future investigations; it is more demanding only in computational power.

The numerical analysis of debonding at interfaces has been carried out by several authors, for example, Lo et al. (1994), Needleman (1987, 1990), Narasimhan (1994), Xu and Needleman (1994), Yeh (1992) through two basic approaches: One is the so-called nodal release technique (Lo et al., 1994, Narasimhan, 1994), the other employs interface elements. The nodal release technique, though more frequently used, permits only a single node to be released at a time by reducing the reaction force at the crack tip node over several time steps and requires continual external monitoring and interruption of the regular finite element computation. In addition, the crack propagation path or debonding path has to be prescribed or tracked node by node which makes the application of the techniques in cases such as debonding at multiple particles rather complicated.

Interfacial constitutive relations and interface element, on the other hand, can treat debonding at interfaces automatically. The present approach is similar to that of Needleman (1987). The main numerical challenges in the present work are that (1) the interfacial failure process in filled-elastomers is usually less stable than that in other types of particulate composites because of the relatively soft matrix (Zhong and Knauss, 1997) and (2) The local instability together with very large strains occur at the interfaces (tens to several hundred percent) raises convergence questions.

In the sequel, we delineate in Section 2 the interface model along with the associated stability issue. The computational

model is presented in Section 3 including the FEM formulation for hyperelasticity and the interface element. Numerical results are demonstrated in Section 4 for unit cell problems,² to evaluate effects of inclusion (particle) size, shape and orientation, as well as of boundary loading and constraints on the response of a unit cell. In solid propellants, particle sizes vary randomly in a range, and they are statistically distributed (Gonzalez and Knauss, 1997). To account for this, we also analyze multi-cell problems, considering interactions among inclusions of identical or different sizes. Additional numerical issues are discussed in Section 5 ending with conclusions in Section 6.

2 An Interfacial Constitutive Model

To imitate the failure behavior of cohesive interface material, the interfacial traction is assumed to increase with increasing interfacial separation to a critical value, after which the traction decreases with increasing separation and eventually vanishes, corresponding to total separation. We take here a damage mechanics point of view by assuming that the interface will lose its stiffness as interfacial separation reaches this critical value (cf Ungsuwarungsri and Knauss, 1987).

2.1 The Interfacial Constitutive Model. Let \mathbf{n} be the normal to an interface, and \mathbf{s} , \mathbf{t} the corresponding orthogonal tangential directions; E_n , E_s and E_t are elastic moduli of a nonlinear (dissipative) spring in the directions $(\mathbf{n}, \mathbf{s}, \mathbf{t})$. The spring response is

$$\mathbf{D} = \begin{bmatrix} E_n^0 & 0 & 0 \\ 0 & E_s^0 & 0 \\ 0 & 0 & E_t^0 \end{bmatrix}, \quad (1)$$

as long as the normal separation Δu_n is less than the critical normal separation Δu_c . When $\Delta u_n > \Delta u_c$, the spring moduli degrade according to

$$\mathbf{D} = \begin{bmatrix} E_n^0 \left(2 - \frac{\Delta u_n}{\Delta u_c} \right) & 0 & 0 \\ 0 & E_s \left(2 - \frac{\Delta u_n}{\Delta u_c} \right) & 0 \\ 0 & 0 & E_t \left(2 - \frac{\Delta u_n}{\Delta u_c} \right) \end{bmatrix} \quad (2)$$

for $\Delta u_c < \Delta u_n \leq 2\Delta u_c$, and vanish for $\Delta u_n > 2\Delta u_c$.

The nonlinear interface constitutive relation is thus

$$\mathbf{f} = \mathbf{D} \Delta \mathbf{u}_{(ns)}, \quad (3)$$

with $\Delta \mathbf{u}$ the relative displacement in local coordinates $(\mathbf{n}, \mathbf{s}, \mathbf{t})$ and \mathbf{f} the conjugate interfacial traction defined in the undeformed reference configuration.

Only failure due to normal separations is accounted for in the current model. Obviously one needs to consider shear failure at an interface for more general situations. It is not difficult to include shear failure into the above interfacial model; see for example Tvergaard and Hutchinson (1993). However, for the type of problems under consideration, the shear strength of the interface is much larger than the tensile strength, so that we do not consider the shear mode failure in the present work.

2.2 Stability of an Interfacial Failure Process Suo et al. (1992) investigated the stability of solids containing interfaces by considering two semi-infinite solids bonded along a

² We use this term frequently to refer to 1-inclusion problems (in finite domains) for notation convenience, even though the analysis does not always impose periodic boundary conditions that belong to a real cell.

planar interface by defining the instability of the system in terms of the onset of nonunique solutions to the associated boundary-value problem. Zhong and Knauss (1997) have recently studied the stability of finite solids, with planar or circular interfaces under homogeneous decohesion (i.e., the whole interface debonds uniformly at the same time), deriving stability criteria for a general form of the traction-displacement interfacial relation

$$f = f(\Delta u). \quad (4)$$

For homogeneous decohesion at a bi-material planar interface the stability condition is

$$\frac{2E_{\text{eff}}}{L} \geq \text{MAX}_{0 < \Delta u < \Delta u_s} \left(-\frac{df}{d\Delta u} \right) \quad (5)$$

where Δu_s corresponds to total separation at the interface. The right-hand side of inequality (5) represent the maximum value of $-(df/d\Delta u)$ when Δu is in $(0, \Delta u_s)$. It is clear that the size of the specimen (L), effective elastic modulus ($E_{\text{eff}} = E_1 E_2 / (E_1 + E_2)$), where E_1 and E_2 are the elastic moduli of the two materials) and the unloading part of the interfacial relation (4) determine the stability of the system. A similar stability condition is obtained for a circular interface (see Zhong and Knauss, 1997).

An interfacial failure process associated with inhomogeneous decohesion at interfaces is intuitively more stable than that associated with a homogeneous decohesion. This is so because the surrounding, bonded regions tend to stabilize the decohesion process. Thus the stability conditions obtained by Zhong and Knauss (1997), though applied only to homogeneous decohesion at interfaces, provide conservative estimates for the onset of instability in an interfacial failure process. It is also clear from the above stability condition (5), that the more compliant the matrix material, the less stable the corresponding composite is under interfacial failure. Thus particulate-filled elastomers tend to be less stable than particulate metallic composites with respect to the interfacial failure process.

It should be noted here that the instability due to interfacial decohesion is local because of the sudden drop of tractions at the interfaces. This local instability poses a problem for the numerical simulation in a quasi-static setting because it can (and does) lead to the divergence of numerical computations.

3 Formulation of the Computational Model

We treat the matrix as a hyperelastic material characterized by a 3-term Ogden strain energy function for finite deformations. For reference purpose, we summarize the hyperelasticity theory and its hybrid FEM formulation briefly.

3.1 Hyperelasticity and Its FEM Formulation. Let Ω_0 be the undeformed reference configuration of the hyperelastic material(s), Ω_t the current deformed configuration, and V_0 and V_t the corresponding volumes. $\mathbf{X} \in \Omega_0$, $\mathbf{y} \in \Omega_t$. Then

$$\mathbf{y} = \mathbf{X} + \mathbf{u}(\mathbf{X}), \quad \mathbf{F} = \frac{\partial \mathbf{y}}{\partial \mathbf{X}}, \quad J = \det(\mathbf{F}). \quad (6)$$

Here $\mathbf{u}(\mathbf{X})$ is the displacement vector at material point \mathbf{X} , \mathbf{F} the corresponding deformation gradient and J the unit volume change.

Because the hyperelastic material is (almost) incompressible, the deformation gradient \mathbf{F} is multiplicatively decomposed into its deviatoric and dilatational parts for purpose of the FEM formulation.

$$\mathbf{F} = \mathbf{F}^{\text{dev}} \mathbf{F}^{\text{vol}}, \quad \mathbf{F}^{\text{dev}} = J^{-1/3} \mathbf{F}, \quad \mathbf{F}^{\text{vol}} = J^{1/3} \mathbf{I}, \quad (7)$$

with \mathbf{I} the identity tensor. It is easy to check that $\det(\mathbf{F}^{\text{dev}}) = 1$, $\det(\mathbf{F}^{\text{vol}}) = J$ so that \mathbf{F}^{dev} is the volume preserving part of \mathbf{F} , and \mathbf{F}^{vol} its dilatation part.

The strain energy function for a nearly incompressible hyperelastic material is expressed as (Ogden, 1984),

$$W(\mathbf{F}) = \bar{W}(\mathbf{F}^{\text{dev}}) + \phi(J), \quad (8)$$

where \bar{W} accounts for the deviatoric deformation and ϕ with $\phi(1) = 0$, for dilatational deformation.

Considering frame indifference, and further assuming that the hyperelastic material is isotropic, we have

$$W(\mathbf{F}) = \omega(\tilde{\lambda}_1, \tilde{\lambda}_2, \tilde{\lambda}_3) + \phi(J), \quad (9)$$

where $\tilde{\lambda}_i$ are the principal deviatoric stretches.

Ogden (1972) assumes that ω has the form (1972),

$$\omega(\tilde{\lambda}_1, \tilde{\lambda}_2, \tilde{\lambda}_3) = \sum_{i=1}^N \frac{2\mu_i}{\alpha_i^2} (\tilde{\lambda}_1^{\alpha_i} + \tilde{\lambda}_2^{\alpha_i} + \tilde{\lambda}_3^{\alpha_i} - 3) \quad (10)$$

so that the initial shear modulus is $\mu_0 = \sum_{i=1}^N \mu_i$ and the relation between Cauchy stress and the principal stretch is

$$\tau_i = \tilde{\lambda}_i \frac{\partial W}{\partial \tilde{\lambda}_i} - \left(\frac{1}{3} \sum_{i=1}^N \tilde{\lambda}_i \frac{\partial W}{\partial \tilde{\lambda}_i} - J \frac{\partial \phi(J)}{\partial J} \right). \quad (11)$$

If the material is fully incompressible ($J = 1$), we have $\phi(J) = 0$, and the corresponding stress-stretch relation is

$$\tau_i = \lambda_i \frac{\partial W}{\partial \lambda_i} - P_i \quad (12)$$

where P_i is an arbitrary pressure and λ_i are the principal stretches.

For almost incompressible material, the usual displacement finite element formulation can behave poorly because the effective bulk modulus is very large compared to its shear modulus, which cause the stiffness matrix to be almost singular from a numerical point of view. Consequently, the stress calculated at the numerical integration points show large oscillation in the pressure. To avoid this, a hybrid element or mixed formulation has been proposed (see for example, Simo and Taylor, 1991). Although extra (pressure or compressibility) variables are introduced in the mixed formulation, the effective degree of freedom at each node in the final FEM formulation are determined by displacements only, because the extra variables are eliminated at the element level.

3.2 Interface Element. The interfacial constitutive relation is implemented by constructing an interface element via the principle of virtual work (Beer, 1985): (1) Set up local coordinates $(\mathbf{n}, \mathbf{s}, \mathbf{t})$ to describe the interface geometrically. (2) Find the relative displacements at the interface in local coordinates. (3) Use the principle of virtual work and the interfacial constitutive relation to obtain an equilibrium equation for the interface element in terms of global nodal coordinates. One then assembles the interface element stiffness matrix with remaining element stiffness matrixes to form the global stiffness matrix.

Drawing on the interfacial constitutive relation and the principle of virtual work, we have

$$\int_{\text{interface}} \mathbf{B}^T \mathbf{f} ds = \mathbf{F}^e, \quad (13)$$

or

$$\int_{\text{interface}} \mathbf{B}^T D \mathbf{B} a ds = \mathbf{F}^e, \quad (14)$$

with \mathbf{F}^e the force vector for nodes of the interface element, \mathbf{a} is the element displacement vector and \mathbf{B} the transformation matrix between nodal displacements and displacement in the

local coordinates. The residual force due to the interface element is

$$R = - \int_{\text{interface}} B^T D_n^{(k)} B ds a_n^k \quad (15)$$

and the tangent stiffness matrix of the interface element is

$$K_t = - \frac{\partial R}{\partial u} \quad (16)$$

Here n refers to time steps, k refers to the sequence of iterations.

For the interfacial relation (3), the tangent stiffness matrix for interface elements is nonsymmetric. Thus using the tangent stiffness matrix may be a source of numerical difficulty.

We use direct iteration, which is expressed for the interface elements by

$$\begin{aligned} \int_{\text{interface}} B^T D_n^k B ds \{ \Delta a \} \\ = F_n^{(k+1)e} - \int_{\text{interface}} B^T D_n^k B ds \{ a_n^k \} \end{aligned} \quad (17)$$

where $a_n^{(k+1)} = a_n^k + \Delta a$, n is the time step, k is the iteration index. The implementation of the FEM formulation for hyperelasticity is available in ABAQUS 5.5. We incorporate the interface element (interfacial constitutive model) into ABAQUS via a user subroutine (user element). It should be noted that the interface element has zero thickness initially.

4 Numerical Results

We consider plane strain deformation of the "particulate" composites. By preliminary choice the parameters in the Ogden function are determined from fitting experimental data of Treloar (1940). The parameters are $\mu_1 = 58.23$, $\alpha_1 = 1.029$, $\mu_2 = 1.35 \times 10^{-5}$, $\alpha_2 = 10.707$, $\mu_3 = 0.246$, $\alpha_3 = -2.957$. They satisfy the material stability condition. The parameters in the interfacial model are also determined quite arbitrarily for now, except that we choose the parameters such that the maximum f_n at an interface is of the same magnitude as that observed in relevant uniaxial tensile experiments (Vratsanos and Farris, 1993). The specific parameter values chosen are $E_n = 10^3$ MPa, $E_t = 10^4$ MPa and $\Delta u_c = 10^{-5}$ m unless specified otherwise.

A 4-node bilinear hybrid element with two effective degrees of freedoms (u , v) is used, along with the interface element described in Section 3.2. The numerical integration of the interface element stiffness matrix is carried out by a 2-point Gaussian quadrature. Due to the instability of the debonding process, all the numerical examples are displacement controlled.

To validate the numerical scheme and to gain insight into the behavior of composites undergoing the evolution of microdamage, we analyze several problems. First, computations are carried out for unit-cell problems to evaluate the influence of bond quality, the effect of the inclusion size (volume fraction), shape and orientation, as well as the boundary loading and constraints. Second, the interaction between multiple inclusions of identical or different sizes is investigated.

In the following, stress refers to Cauchy stress if not specified otherwise, strain connotes nominal strain.

4.1 Uniaxial Stretching of an Elastomer Containing a Circular Inclusion. A 3 mm \times 3 mm square elastomer element containing a circular inclusion (radius 1.3 mm, volume fraction 59 percent) is analyzed in a sequence of displacement controlled deformations. In all cases, the boundary condition is mixed, i.e., a constant normal displacement is prescribed on two opposite sides and the remaining two sides are traction free.

First the "global" stress-strain behavior of the element is compared for different bond qualities at the interface, namely unbonded, perfectly bonded and bonded according to the interfacial relation (3). These overall stress-strain responses are

also compared with that of a pure elastomer square and that of an elastomer square with a hole of radius 1.3 mm at the center.

Figure 2 illustrates the global stress-strain response of a single element with and without an inclusion. As expected one notes that compared to pure elastomer, the configuration with a perfectly bonded inclusion is stiffer and that with a hole is softer than the pure elastomer. In addition one observes that the element with a bonded inclusion loses stiffness gradually as the debond increases, and becomes more compliant than the pure elastomer. Also one observes that when a large area is debonded, the geometry behaves like one with an unbonded inclusion. The largest nominal strain is in the order of 600 percent.

4.2 Effect of Inclusion Size. The effect of inclusion size in a unit-cell is considered next and documented in Fig. 3 for inclusion radii of $r = 0.25, 0.5, 1.0, 1.3$ mm in an initial domain of 3 mm \times 3 mm (Corresponding volume fractions are 2.2, 8.7, 35.0, 59.0 percent). When the size of inclusion is small (0.25 mm, 0.5 mm, 1 mm) relative to the domain size, the overall stress-strain curve is monotonic; when the size of the inclusion is large (1.3 mm), the overall stress-strain trace is not. The larger the inclusion size, the sooner the specimen debonds and loses stiffness, because debond initiation occurs earlier for the larger inclusion. When the inclusion size is very small (0.25 mm), the stiffness of the composite element is larger than that for pure elastomer even when debonding occurs.

4.3 Change of Boundary Constraints. To check the effect of boundary conditions on the overall behavior of a unit-cell (volume fraction 35 percent), we change the boundary conditions at the "sides" of the unit cell from traction free, to (a) elastic foundation (i.e., the side walls of the unit cell are constrained horizontally by springs), (b) zero normal displacement ($u_1 = 0$). The behavior of the unit-cell changes noticeably (Fig. 4): over the strain range presented, the traction free condition leaves part of the bond between the matrix and inclusion intact, while the lateral displacement constraint leads to early dewetting closely followed by the elastic constraint, but with somewhat later unbonding.

4.4 Effect of Inclusion Shape and Orientation. Inclusions are generally not round. The effect of the shape of an inclusion is investigated by considering inclusions in the shape of a circle, an ellipse and a square located in the center of a square elastomer matrix. The shape of an inclusion affects the time of debond initiation and the growth of voids (detail results not reported here).

The orientation effect is investigated by considering a specimen with an elliptic inclusion (aspect ratio 2, volume fraction

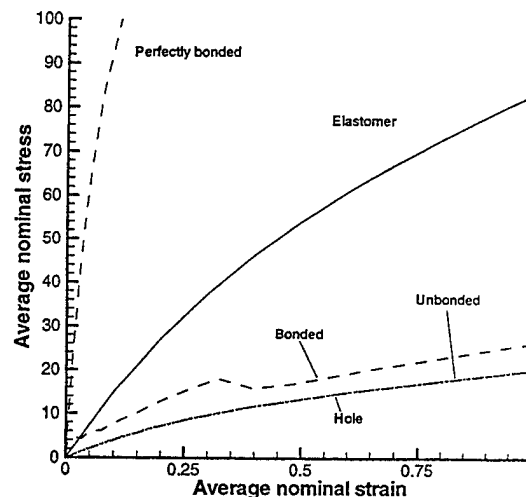


Fig. 2 Evaluation of bond qualities: overall stress-strain curves

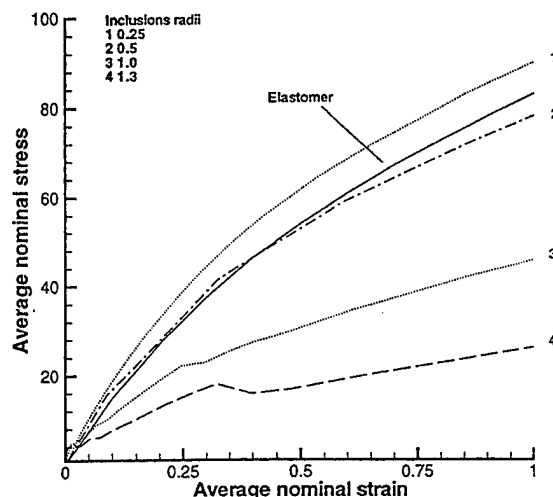


Fig. 3 Effect of inclusion sizes

17.5 percent) in three orientations (major axis is oriented 90, 45 and 0 degrees with respect to the tension axis). Figure 5 shows that when the elliptic inclusion is oriented at 90 or 45 degrees, the overall stress-strain curves are non-monotone. For the 90 deg case, the debonding occurs over a large portion of the interface almost at once, which corresponds to the drop in stress in Fig. 5 (curve 3). A similar situation arises for the 45 deg case. These indicate that when the largest cross section of the inclusion is perpendicular to the loading axis, the debonding occurs earlier and faster than for (near) alignment.

4.5 Interaction of Inclusions. A comparison was also made between different numbers of inclusions in a block of elastomer which have the same volume fraction and identical inclusions. The number of inclusions considered are 1, 2, and 4. It is observed that there is basically no difference between the case of one inclusion and that with two inclusions. The overall stress-strain curve for the elastomer with four inclusions differs little from those with one or two inclusions, and there is a trend that the overall stress-strain curve converges to a single curve as the number of inclusions increases.

A square elastomer with 4 and 16 inclusions was also considered for which the inclusion sizes fluctuate around a mean value (0.3 mm for the 4-inclusion case, 0.4 mm for the 16-inclusion case). Again, normal displacements are described at two opposite sides of the elastomer. The remaining two sides are traction

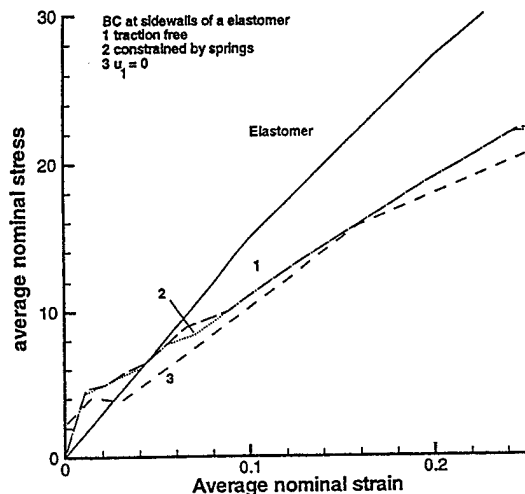
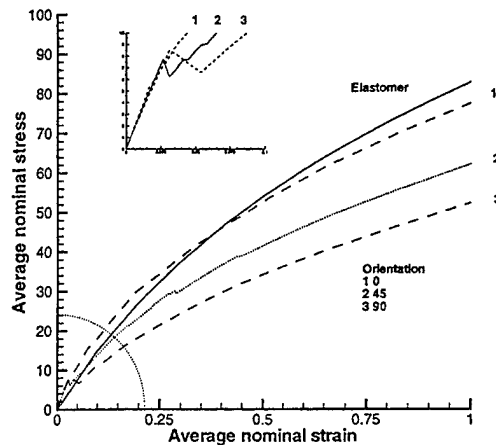
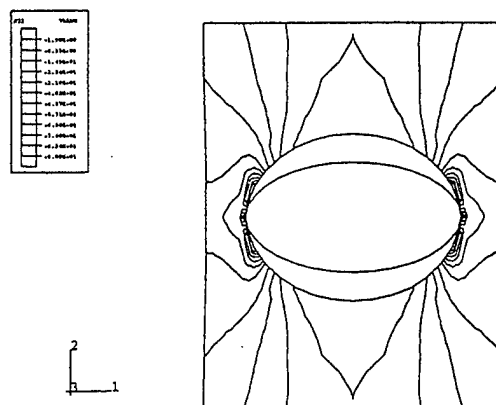


Fig. 4 Effect of changing boundary constraints



(a)

Fig. 5(a)



(b)

Fig. 5(b)

Fig. 5 Effect of orientations: (a) the overall stress-strain curves; (b) a stress contour

free. The size of the elastomer is 2 mm \times 2 mm for the 4-inclusion case, and 4 mm \times 4 mm for the 16-inclusion case. For the 4-inclusion case, the computation extends to 18.3 percent overall strain (the largest normal strain in the elastomer is 43 percent), after which it diverges. For the 16-inclusion case the computation reaches 4 percent overall strain with the largest normal strain being 23 percent, thereafter the algorithm diverges (see Fig. 6).

A more detailed examination of the results for the two cases shows that debonding occurs first at the larger inclusions and voids formed there grow larger as the external load increases compared to those at smaller inclusions. The voids formed at smaller inclusions seem not to grow or grow very slowly. This is consistent with the observation made in the unit-cell situation. What cannot be observed in a unit-cell setting is that the voids formed at the inclusion-matrix interface can grow, they can also shrink as external loading is increased due to the interaction among inclusions (see Fig. 7), and that a sufficiently large void tends to coalesce with a sufficiently large nearby void, but not necessarily the nearest void. In addition discrete segmental increases are observed in the overall stress-strain curve for the 16-inclusion case, but not for the 4-inclusion case, this is due to the fact that the 16-inclusion case has a larger volume fraction of inclusions than the 4-inclusion case (about 50 percent versus 30 percent). This "roughness" in the stress-strain response has also been observed by Gonzalez and Knauss (1997), where the

volume fraction of (three-dimensional) particles is about 70 percent.

5 Some Numerical Issues

It is observed that the convergence of computations is very sensitive to the mesh, time increment and quadrature for the integration of the interface element stiffness matrix. When debonding occurs, a very large number of iterations is necessary. We tested Gaussian quadrature and Lobatto quadrature for the integration of the interface element. In the present, large deformation occasion, Gaussian quadrature was found more satisfactory than Lobatto quadrature, which is more efficient in cases of small matrix deformation (see, for example, Schellekens and De Borst, 1993).

In order to analyze a force-controlled problem setting or an unstable failure process in a displacement controlled problem setting, a dynamic rather than a quasi-static formulation is needed. The interfacial decohesion propagates very rapidly during an unstable failure process as observed by Gonzalez and Knauss (1997). The unstable nature of a fast propagating decohesion also shows up in stress-strain curves as a small, sudden drop in the stress.

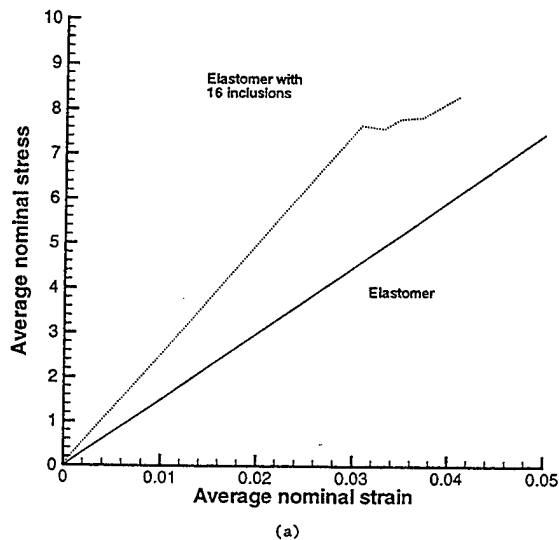


Fig. 6(a)

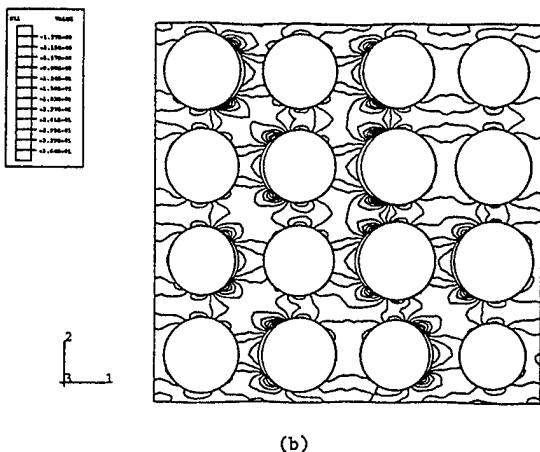


Fig. 6(b)

Fig. 6 Interaction of (16) inclusions of different sizes: (a) the overall stress-strain curve; (b) a stress contour

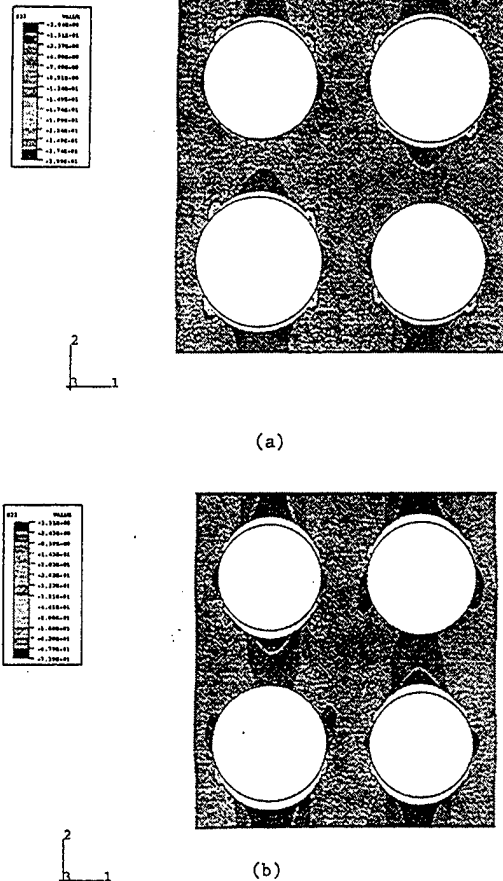


Fig. 7 A 4-inclusion case: voids formed at interfaces can grow and/or shrink when external load increases (a) overall strain 8.6 percent; (b) overall strain 18.3 percent

6 Conclusions

By characterizing the particles, matrix and interfaces in a particulate-filled elastomer individually, the whole failure process (interfacial debonding, growth of voids formed at interfaces) is analyzed by the FEM. It is demonstrated that the scheme can predict the damage evolution in particulate-filled elastomer in a "discontinuum" way. The predictions are qualitatively the same as those observed in laboratory experiments.

The main observations are that the behavior of particulate-filled elastomers depends on the size, shape, orientation and interface properties: in an elastomer containing regularly distributed identical particles, the overall stress-strain curve seems to converge to a single curve as the number of particles increases (fixed volume fraction); in a filled-elastomer containing different size particles, the interaction among particles plays an important role in the growth and coalescence of voids. The interfacial failure process is highly unstable, especially when the volume fraction of inclusions is relatively large.

In order to analyze more complicated problems, such as interaction of particles and a macroscopic crack, propagation of a crack via the growth and coalescence of voids, the computational approach must be made more robust and stable.

Acknowledgment

The work reported here has been supported by AFOSR. We benefited from discussions with Dr. C. T. Liu of Phillips Laboratory, Edwards Air Force Base, and with Prof. M. Ortiz on numerical techniques. We are grateful to Hibbitt, Karlsson & Sorensen, Inc. for making available the ABAQUS finite element

code to us under an academic license. We are also grateful to NSF/UCSD San Diego Supercomputer Center where part of the computations were carried out.

References

- Barenblatt, G. I., 1962, "Mathematical Theory of Equilibrium Cracks," *Adv. App. Mech.*, Vol. 7, 56-129.
- Beer, G., 1985, "An Isoparametric Joint/Interface Element for Finite Element Analysis," *Int. J. Num. Methods Eng.*, 21, 585-600.
- Dugdale, D. S., 1960, "Yielding of Steel Sheets Containing Slits," *J. Mech. Phys. Solids*, 8, 100-104.
- Farris, R. J., 1964, "Dilatation of Granular Filled Elastomers Under High Rates of Strain," *J. Appl. Polym. Sci.*, 8, 25-35.
- Farris, R. J., and Schapery, R. A., 1973, "Development of a Solid Rocket Propellant Nonlinear Viscoelastic Theory," Technical Report AFRPL-TR-73-50, Air Force Rocket Propulsion Laboratory, Edwards, CA.
- Gent, A. N., and Park B. 1984, "Failure Progresses at or Near a Rigid Spherical Inclusion," *J. Mater. Sci.*, 19(6), 1947-1956.
- Govindjee, S., and Simo, J. C., 1992, "Transition From Micromechanics to Computationally Efficient Phenomenology: Carbon Filled Rubbers Incorporating Mullins Effect," *J. Mech. Phys. Solids*, 40, 213-233.
- Gonzalez, J., and Knauss, W. G., 1997, "Full Field Study of Strain Distribution Near the Crack Tip in Fracture of Solid Propellant Via Large Strain Digital Image Correlation and Optical Microscopy," submitted to *Experimental Mechanics*, also Caltech thesis (1996).
- Knauss, W. G., and Mueller, H. K., 1979, "Polymer Reinforcement From the Viewpoint of Fracture Mechanics," *Composite Materials*, G. S. Sih and V. P. Tamuzs, Eds., Sijthoff and Noordhoff.
- Liu, C. T., 1991, "Evaluation of Damage Fields near Crack Tips in a Composite Solid Propellant," *J. Spacecraft and Rockets*, 28(1), 64-70.
- Lo, C. Y., Nakamura, T., and Kushner, A., 1994, "Computational Analysis of Dynamic Crack Propagation Along a Bimaterial Interface," *Int. J. Solids Structures*, 31(2), 145-168.
- Narasimhan, R., 1994, "A Numerical Studies of Fracture Initiation in a Ductile Population of 2nd Phase Particles, 1. Static Loading," *Engineering Fracture Mechanics*, 47(6), 919-934.
- Needleman, A., 1987, "A Continuum Model for Void Nucleation by Inclusion Debonding," *ASME J. App. Mech.*, 54, 525-531.
- Needleman, A., 1990, "An Analysis of Decohesion Along an Imperfect Interface," *Int. J. Fracture*, 42, 21-40.
- Oberth, A. E., 1967, "Principle of Strength Reinforcement in Filled Rubbers," *Rubber Chem. Technol.*, 40, 1337-1363.
- Ogden, R. W., 1972, "Large Deformation Isotropic Elasticity: On the Correlation of Theory and Experiment for Incompressible Rubber Like Solids," *Proc. R. Soc., London A*, 326, 565-584.
- Ogden, R. W., 1984, *Non-Linear Elastic Deformation*, Ellis Horwood Limited.
- Ravichandran, G., and Liu, C. T., 1995, "Modeling Constitutive Behavior of Particulate Composites Undergoing Damage," *Int. J. Solids Structures*, 32(6/7), 979-990.
- Schellekens, J. C. J. and De Borst, R., 1993, "On the Numerical Integration of Interface Elements," *Int. J. Num. Methods Eng.*, 36, 43-66.
- Schapery, R. A., 1986, "A Micromechanical Model for Nonlinear Viscoelastic Behavior of Particle-Reinforced Rubber With Distributed Damage," *Eng. Fract. Mech.*, 25, 845-867.
- Schippel, H. F., 1920, *Ind. Eng. Chem.*, 12, 33-???
- Simo, J. C., and Taylor, R. L., 1991, "Quasi-incompressible Finite Elasticity in Principle Stretches: Continuum Basis and Numerical Algorithms," *Computer Methods in App. Mech. and Eng.*, 85, 273-310.
- Smith, T. L., 1959, "Volume Changes and Dewetting in Glass Bead- Polyvinyl Chloride Elastomeric Composites Under Large Deformations," *Trans. Soc. Rheology*, III, 113-136.
- Suo, Z., Ortiz, M., and Needleman, A., 1992, "Stability of Solids with Interfaces," *J. Mech. Phys. Solids*, 40(3), 613-640.
- Tvergaard, V., and Hutchinson, J. W., 1993, "The Influence of Plasticity on Mixed Mode Interface Toughness," *J. Mech. Phys. Solids*, 41(6), 1119-1135.
- Treloar, L. R. G., 1940, "Stress-Strain Data for Vulcanised Rubber Under Various Deformation," *Trans. Faraday Soc.*, 40, 59-70.
- Ungsuwarungsri, T., and Knauss, W. G., 1987, "The Role of Damage- Softened Material Behavior in the Fracture of Composites and Adhesives," *Int. J. Fracture*, 35, 221-241.
- Vratsanos, L. A., and Farris, R. J., 1993, "A Predictive Model for the Mechanical Behavior of Particulate Composites. Part I: Model Derivation," *Polymer Eng. Sci.*, 33(22), 1458-1474.
- Xu, X. P., and Needleman, A., 1994, "Numerical Simulations of Fast Crack Growth in Brittle Solids," *J. Mech. Phys. Solids*, 42, 1397-???
- Yeh, J. R., 1992, "The Effect of Interface on the Transverse Properties of Composites," *Int. J. Solids Structures*, 29(20), 2493-2502.
- Zhong, X., and Knauss, W. G., 1997, "A Simple Consideration of the Dewetting Instability in a Finite Solid With Interfaces," ASME/ASCE/SES joint summer meeting, McNU'97, Northwestern University.
- Zubelewicz, A. and Bazant, Z. P., 1987, "Interface Element Modeling of Fracture in Aggregate Composites," *J. Eng. Mech.*, 113(11), 1619-1630.
- ABAQUS Manuals (version 5.5), Hibbitt, Karlsson & Sorensen, Inc.

**ON THE STABILITY OF PHASE SEPARATION
IN A FINITE SOLID WITH INTERFACES**

X. Allan Zhong and Wolfgang G. Knauss
Graduate Aeronautical Laboratories, Mail Code 105-50
California Institute of Technology
Pasadena, CA 91125, USA

RUNNING HEAD: STABILITY OF PHASE SEPARATION

Corresponding author: X. Allan Zhong

105-50 Caltech

Pasadena, CA 91125

Tel: 626-395-4527, Fax: 626-304-0175

e-mail: allan@atlantis.caltech.edu

Submitted to Mechanics of Composite Materials and Structures

SUMMARY

The stability of homogeneous phase separation in finite solids containing planar, cylindrical or spherical interfaces is investigated analytically. Explicit stability conditions are deduced for each interface geometry. It is shown how the interaction of load (force or displacement), material properties of the phases and interface properties jointly determine the stability of the interface separation process.

INTRODUCTION

In an effort to model failure and fracture in highly particle filled solids (solid propellant rocket fuels for example) it has been proposed to characterize the damage in the crack tip region through discretized representation of the deformations around particles, including their separation from binder, which is usually referred to as "dewetting" (Zhong and Knauss [1]). The extent of the region in which this phenomenon needs to be modeled in detail is determined experimentally to be on the order of a millimeter or a fraction thereof. Outside this domain the composite is to be described by a (possibly nonlinear) continuum constitutive law. Thus the individual phases of the composites are characterized separately, i.e. matrix material, particles and the interfaces are assigned different constitutive behavior in a detailed finite element model.

In evaluating such models for various phase properties and volume fractions, instabilities occur that raise the question whether their origins are numerical or physical in nature. Since interfaces are ubiquitous in (fibrous, particulate or layered) composites and damage accrued through interfacial failure is an important phenomenon in these solids, we address the issue how the interaction of specimen size, filler geometry, properties of matrix and interfacial constitution lead to stable vis-à-vis unstable interfacial separation. It thus the purpose of this note to illuminate this question through deriving global criteria

that establish conservative estimates for the onset of instability. In the context of layered, fibrous and particulate composites we consider thus finite domains containing planar, cylindrical or spherical interfaces.

Interfaces can be characterized at least qualitatively by interfacial constitutive models (see for example, Needleman [2], Ungsuwarrungsri and Knauss [3]). Suo, Ortiz and Needleman [4] investigated the stability of solids containing interfaces in terms of two semi-infinite solids bonded along a plane by defining the onset of instability as the appearance of non-unique solutions to the associated boundary-value-problem. In the sequel, the principle of minimum potential energy is used to select a favorable solution when bifurcation occurs. The unstable solution is considered in the Liapunov sense such that an infinitesimal change in the excitation produces a finite change in response. It is shown that the onset of non-uniqueness of solutions to boundary values problems does not necessarily lead to instability in an energy sense, a result that includes the special situation of a propagation craze-crack employing more specific interfacial constitutive descriptions (Ungsuwarungsri and Knauss [5]).

Stability analyses for the development of inhomogeneous deformation fields have been performed in connection with shear band formation when coupled with material strain softening behavior as (in the absence of any fracture), for example, by Needleman [6]. More recently Levy [7] has studied how phase concentration affects stability through a bifurcation condition in a two dimensional setting and for a specific interface model. Here we consider a more general model of interface cohesion, and identify how the interaction of load (displacement or force), matrix material properties and interface properties jointly determine the stability of an interfacial separation process. We show specifically that interfacial separation instability involves the maximum negative slope of the unloading portion of the interface cohesion model together with the matrix modulus and the

specimen size. Thus the work reported here provides new perspectives for numerical simulation of interfacial failure process.

AN INTERFACIAL CONSTITUTIVE MODEL

Interfacial constitutive models considered to date are typically rate independent and relate the separation to the traction across an interface. The general features of these models are that the traction across the interface first increases and then decreases with interfacial separation; by definition total separation at the interface is achieved when the traction across the interface has dropped to zero. For bond-normal separation, an interfacial constitutive relation between the traction T and separation Δ

$$T = f(\Delta) \tag{1}$$

is illustrated schematically in Figure 1.

A PLANAR INTERFACE

Consider an elastic two-phase solid consisting of two rectangular plates (with Young's modulus and Poisson's ratios E_1, ν_1, E_2, ν_2) bonded as shown in Figure 2. The interface is vanishing thin and is characterized by the interfacial constitutive relation of the form described in Figure 1. Because the system obviously becomes unstable as soon as $T = \sigma_{\max}$, if normal traction \underline{t} are prescribed at $x_2 = \pm L$. We consider here only a displacement control problem with boundary conditions

$$\underline{t} = 0, \quad \text{at } x_1 = 0, a,$$

$$t_1 = 0, u_2 = \pm \bar{u}, \quad \text{at } x_2 = \pm L.$$

For reasons of simplicity eliminate shear stress by letting $\nu_1 = 0$ and $\nu_2 = 0$. Equilibrium (plane stress) and compatibility determine that the edge displacement \bar{u} , the homogeneous stress $\sigma (= \sigma_{22})$ and the separation Δ at the interface are related by

$$f(\Delta) = \frac{2\bar{E}}{L}(2\bar{u} - \Delta) \quad (2)$$

where $\bar{E} = E_1 E_2 / (E_1 + E_2)$.

This nonlinear algebraic equation can be analyzed geometrically. Consider the intersection of the curve $y = f(\Delta)$ and the straight line(s) $y(\bar{u}, \Delta) = 2\bar{E}(2\bar{u} - \Delta) / L$. The number of solutions to (2) (intersections of the two y-functions) depends on the slope of the straight line(s) and the magnitude of \bar{u} for given interface properties (See Figure 3) : When the slope $(2\bar{E} / L)$ of straight line(s) is sufficiently large, the solution to (2) is unique for all \bar{u} ; for smaller slopes, the solution can bifurcate when \bar{u} is large. Thus the condition for the existence of a unique solution to (2) is thus

$$\frac{2\bar{E}}{L} \geq \max_{0 < \Delta < \Delta_0} (-f'(\Delta)). \quad (3)$$

Let Π be the total energy (work done on) in the system, consisting of the sum of the energy stored elastically in the plates and the work done against the interface traction

$$\frac{\Pi}{a} = \frac{L\sigma^2}{2\bar{E}} + \int_0^{\Delta} f(\xi)d\xi = \frac{L}{2\bar{E}} f^2(\Delta) + \int_0^{\Delta} f(\xi)d\xi, \quad (4)$$

with f given by (2).

When $\frac{2\bar{E}}{L} \geq \max_{0 < \Delta < \Delta_0} (-f'(\Delta))$, the total energy Π of the system is a monotonic function of

the applied displacement \bar{u} ; When $\frac{2\bar{E}}{L} < \max_{0 < \Delta < \Delta_0} (-f'(\Delta))$, and \bar{u} is sufficiently large,

there are two or three solutions to (2). For each solution, the corresponding Π is a monotonic function. The acceptable solution is that which minimize the potential energy.

It is thus seen that when \bar{E}/L is large, a stable homogenous decohesion of the interface is possible in the sense that a continuously varying separation of the interface occurs as a function of the applied displacement; otherwise the instability of the system occurs. This can happen even before the stress at the interface reaches σ_{\max} and the two plates separate suddenly at a non zero stress, provided \bar{E}/L is sufficiently small. In other words, the stiffer the bulk materials and smaller the domain size, the more stable the system is under boundary displacement control.

A CIRCULAR INTERFACE

Consider next a simple case of a cylindrical rod or fiber (assumed rigid) embedded in an elastic cylindrical matrix with inner radius a , outer radius b , possessing an elastic modulus E and Poisson's ratio ν under plane strain conditions, assuming that the rod

(inclusion) is rigid. The interface is again characterized by the interfacial constitutive relation illustrated in Figure 1.

Assuming axisymmetric deformation there are no shear stresses in the system.

The boundary conditions (polar coordinates (r, θ)) are then

$$(I) \quad r = b, u_r = \bar{u}, t_\theta = 0. \text{ (displacement control)}$$

or

$$(II) \quad r = b, t_r = \bar{t}, t_\theta = 0. \text{ (force control)}$$

It is easy to show that the stability conditions for these two boundary conditions are

(1) Displacement control

$$\frac{2Eb(b^2 - a^2)}{(a^2 + b^2)^2(1 - \nu^2)} \frac{b^2(1 - \nu) + a^2(1 + \nu)}{2ab} \geq \max_{0 < \Delta < \Delta_0} (-f'(\Delta)) \quad (5)$$

(2) Traction control

$$\frac{E(b^2 - a^2)\Delta}{a(a^2(1 - \nu) + b^2(1 + \nu))} \geq \max_{0 < \Delta < \Delta_0} (-f'(\Delta)) \quad (6)$$

The potential energy as a function of applied displacement is given as an example in Figure 4 for an unstable decohesion process. Compared with the case for the planar interface, we see that (1) stable interfacial decohesion is possible even the process is force controlled, (2) debonding process is more stable the larger b/a is; this is opposite to the

finding for the planar interface where a smaller “L” corresponds to the more stable debonding process. Thus the stability of interfacial failure (dewetting) depends on the interfacial properties as well as on the geometry of the interface and loading conditions.

A SPHERICAL INTERFACE

A three dimensional generalization of the results for the circular interface case is easily realized by considering a rigid spherical particle ($r = a$) embedded in a spherical domain (bonded by $r = b$) of Young's modulus E and Poisson's ratio ν subjected to axisymmetric deformation. This consideration involves a spherical interface, the geometrically simplest interface in particulate composites.

The boundary conditions (spherical coordinates (r, θ, φ)) are then

$$(I) \quad r = b, u_r = \bar{u}, t_\theta = 0, t_\varphi = 0. \text{ (displacement control)}$$

or

$$(II) \quad r = b, t_r = \bar{t}, t_\theta = 0, t_\varphi = 0. \text{ (force control)}$$

leading to the stability conditions

(I) Displacement control

$$\frac{2(1-2\nu)b^3 + (1+\nu)a^3}{a^3(2(2-\nu)b^3 - (1+\nu)a^3)} \frac{E(b^3 - a^3)}{b - a} \geq \max_{0 < \Delta < \Delta_0} (-f'(\Delta)). \quad (7)$$

(II) Traction control

$$\frac{E(b^3 - a^3)}{a((1 + \nu)b^3 + (1 - 2\nu)a^3)} \geq \max_{0 < \Delta < \Delta_0} (-f'(\Delta)). \quad (8)$$

DISCUSSION

The above stability conditions are consistent with recent numerical experiences (Zhong and Knauss [1], Needleman [8]) for both planar and circular interfaces in much more complex situations. As far as the stability of a system involving homogeneous interfacial decohesion is concerned, there is not much difference between a circular interface and a spherical interface.

The instability is associated to the sudden drop of traction at interfaces and associated energy release when interfacial failure occurs. This local instability poses considerable difficulties for the numerical simulation of interfacial failure in a quasi-static setting and will lead to the divergence of numerical computations. One way to cope with this complication is to model the interfacial failure process as a dynamic process. Another way is to “regularize” the interfacial constitutive relation at the point of the instability onset, replacing the original traction separation curve by a “modifying” line derived from stability analysis. Such a regularization may lead to avoidance of instabilities in numerical computation while retaining the basic feature of the original response. This regularization makes the corresponding numerical simulation somewhat similar to the “nodal release” technique¹.

¹ In this regularization process the fracture energy remains as the same as that defined by the interfacial model while the fracture energy associated with the “nodal release” technique is arbitrary (undefined).

We have considered here only uniform decohesion at interfaces. A more complete description would concern the stability of the local failure process through an inhomogeneous decohesion. Intuitively, an interfacial failure process involving inhomogeneous decohesion is more stable than that involving homogeneous decohesion here, because the surrounding bonded region tends to stabilize the decohesion process. Thus the stability estimation obtained here for homogenous decohesion might provide a non-conservative estimate of the onset of instability for an arbitrary interfacial failure process. It has the advantage of relating in a simple manner the domain size and the properties to a stability criterion, a situation that requires much more analysis for an inhomogeneous dewetting process.

ACKNOWLEDGMENT

This work is supported by AFOSR. We would also like to thank Prof. Jim Knowles for discussions on the subject

REFERENCE

1. Zhong X. and Knauss W. G., An analysis of interfacial failure in particle-filled elastomers, *ASME J. Eng. Materials Tech.*, 119(3), 198-204. (1997)
2. Needleman A., A continuum model for void nucleation by inclusion debonding, *ASME J. App. Mechanics*, 54, 525-531. (1987)

3. Ungsuwarungsri T. and Knauss W. G., The role of damage-softened material behavior in the fracture of composites and adhesives, *Int. J. Fracture*, 35, 221-241. (1987)
4. Suo Z., Ortiz M. and Needleman A., Stability of solids with interfaces, *J. Mech. Phy. Solids*, 40(3), 613-640. (1992)
5. Ungsuwarungsri T. and Knauss W. G., A nonlinear analysis of an equilibrium craze: Part I-Problem solution and formulation, *ASME J. App. Mechanics*, 55, 44-51. (1988)
6. Needleman A., On the competition between failure and instability in progressively softening solids, *Journal of Applied Mechanics (ASME)*, 58, 294-296. (1991)
7. Levy, A. J., The effective dilatational response of fiber-reinforced composites with nonlinear interface, *Journal of Applied Mechanics (ASME)*, 63, 357-364. (1996)
8. Needleman A. (1992), An analysis of decohesion along an imperfect interface, *Int. J. Fracture*, 42, 21-20.

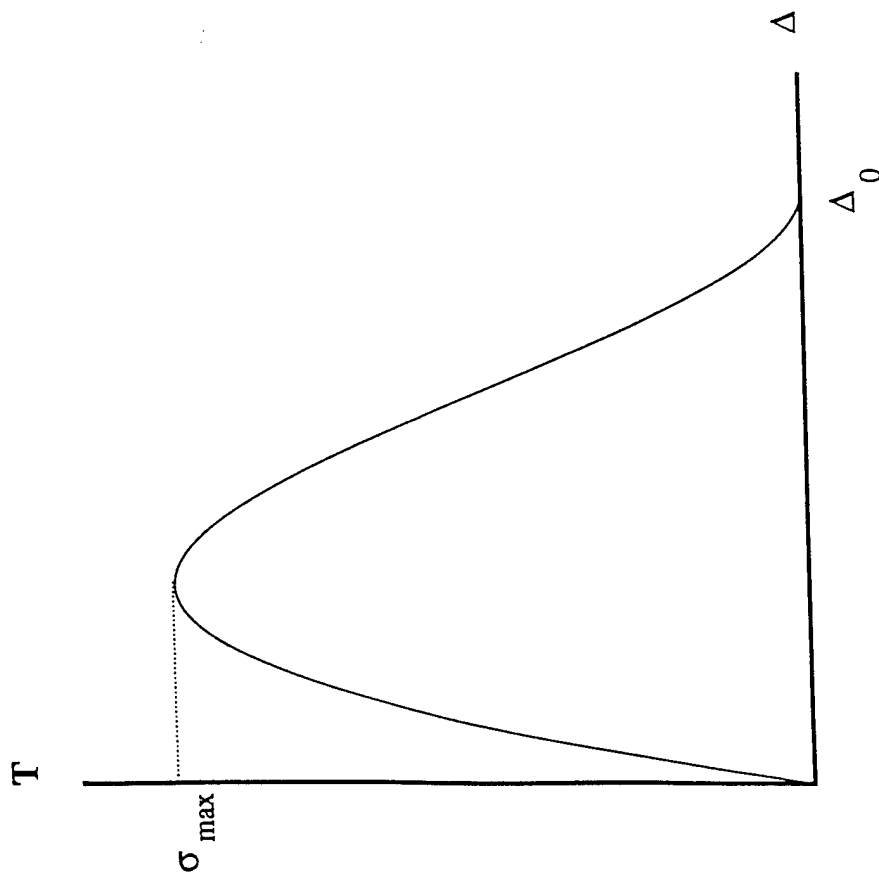


Figure 1. A schematic interfacial constitutive model for normal debonding

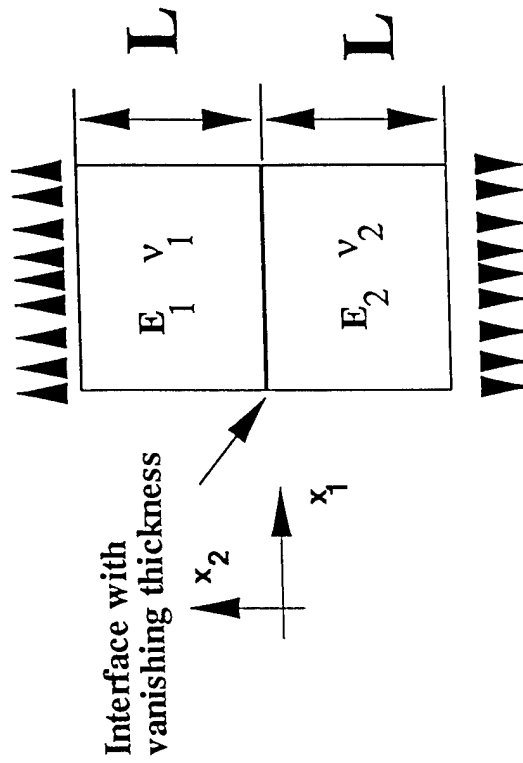


Figure 2. A finite solid with an interface of vanishing thickness

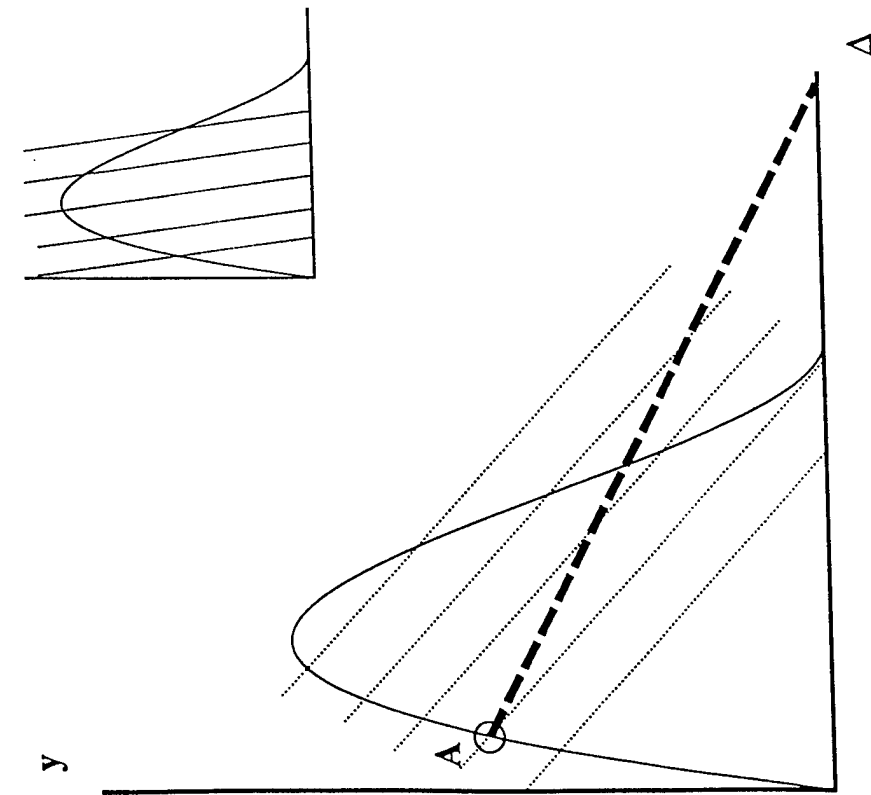


Figure 3. Illustration for the analysis of equation (2)

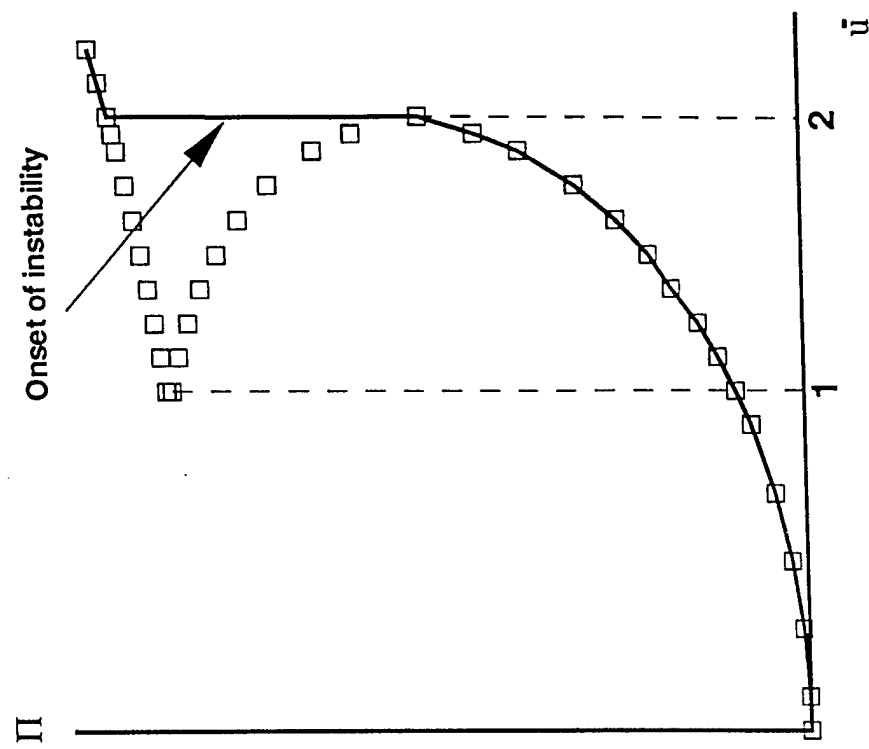


Figure 4. Potential energy vs. applied displacement for an unstable case.

EFFECTS OF PARTICLE INTERACTION AND SIZE VARIATION ON DAMAGE EVOLUTION IN FILLED ELASTOMERS

X. Allan Zhong and Wolfgang G. Knauss

Graduate Aeronautical Laboratories

California Institute of Technology

Pasadena, CA 91125, USA

Abstract

A micromechanical analysis of damage evolution (interfacial debonding) in particle-filled elastomers addresses the effect of the interactions between particles and of variation in filler size. The composite is treated as an assembly of two constituents in a finite element model. It is shown that the interaction between particles controls the damage evolution: (1) For high volume fraction, a relatively small change in particle size has a surprisingly large effect on local material response; (2) for large differences in particle sizes (e.g. bimodal distribution), damage occurs at interfaces between large particles and matrix, with limited damage occurring at small particles. While these effects of particle interaction and size variation are smoothed out in a large ensemble of particles, it is foreseeable that they are an important factor in a failure process such as macroscopic crack propagation, which spans scales considerably larger than the maximum particle size. Specifically, one expects thus that in the vicinity of a macroscopic crack the large particles become sites for small cracks which coalesce to larger ones and join up with the macro crack, while small particles operate primarily so as to locally stiffen the matrix without incurring significant damages in their vicinity.

1 Introduction

Recently substantial efforts have been made in community of mechanics of materials towards damage evolution in composites and its effect on global material behavior. Theoretical stud-

ies with constitutive models accounting for damage have been proposed; see for example, Farris and Schapery (1973), Schapery(1986), Govindjee and Simo (1992), Vratsanos and Farris (1993), and Ravichandran and Liu (1995). By proposing a constitutive model, one implicitly treats a damaged material as a homogenized material and neglects any detailed interaction between various damage sites. In attempts to inquire into the mechanics of the damage development finite element analyses tend to make use of unit-cell models (Needleman (1987), Yeh (1992), and Walter, Ravichandran and Ortiz (1997) in which one assumes that fillers (fibers, particles etc) are uniformly of the same size and (periodically) distributed homogeneously in the composite. However the unit-cell approach cannot address the interaction between particles or their clustering of fillers, nor can it be instructive on the effect of variations in filler size.

The motivation behind the current work is the desire to develop a computational scheme to deal with the fracture behavior of particulate composites. To this end Zhong and Knauss (1997b) have proposed a hybrid discrete-continuum approach which incorporates the discrete damage evolution in filled elastomers. The basic thought is to characterize the material far from the crack tip as a homogeneous body, while close to the crack tip, in a region measured possibly in millimeters or thereof the discrete particulate interaction with damage evolution are modeled as illustrated in Figure 1. Such pursuits appear feasible in light of the ever more rapidly increasing power of computing machines. Initial studies directed to that goal have shown that for small numbers of particles the material behavior is reproduced qualitatively (Zhong and Knauss (1997b)).

In this paper we concentrate on the effect which the interactions of particles have on the damage evolution along with the quest for understanding the role which particle size plays in this picture. For the purpose of this initial study, the elastomer matrix is characterized as a hyperelastic Ogden material (Ogden, 1972), although, in reality, the elastomer may possess time dependent characteristics ¹. Because the elastomer matrix is typically soft relative to the particles, the latter may be considered to be rigid ². The interface between particle and

¹The motivation for this work comes from the failure behavior of solid propellant rocket fuel; these materials possess time or rate dependent properties, but for exploratory purposes, it suffices to ignore the effects.

²This choice is made for convenience. Under high rate loading, the binder may be stiff by compression

matrix can fail and is, therefor, modeled by a cohesive-zone type feature with the bond at the interfaces so "weak" that only interfacial debonding needs to be considered (no cavitation occurs in the elastomer). A two dimensional version of the problem is considered here and a fully three dimensional problem description is left to future investigations, since it requires only a larger/faster computer.

In the sequel we delineate the interface model along with the associated stability issue in Section 2. The computational model is presented in Section 3 including the FEM formulation for hyperelasticity and the interface element. To evaluate the effect of the interaction between particles (inclusions) of different size, we analyze configurations of four (4) as well as sixteen (16) inclusions wherein the particle sizes vary by small amounts (10%). In addition we examine the interaction between inclusions for a bimodal size distribution and find that (1) for a high volume fraction of filler, a small change in particle size has a large effect on material response, (2) when there is a big difference in particle sizes(such as bimodal distribution), damage occurs along interfaces of large particles, little damage taking place around small particles.

2 An interfacial constitutive model

To model the interfacial separation, we imitate the cohesive failure by a traction-displacement relation that replaces the local constitutive behavior in a thin layer (zero thickness in the model). The interfacial traction is assumed to increase with increasing interfacial separation to a critical value, after which the traction decreases with increasing separation, eventually vanishing, which condition then corresponds to total separation. (cf Ungsuwarungsri and Knauss;1987).

2.1 The interfacial constitutive model

Let \mathbf{n} be the normal to an interface, and \mathbf{s} , \mathbf{t} the corresponding orthogonal tangential directions; E_n , E_s and E_t are elastic moduli of a nonlinear (dissipative) spring in the directions so that the particles will also deform. That case is computationally treatable as well, but requires larger computational resources.

$(\mathbf{n}, \mathbf{s}, \mathbf{t})$. The spring response is

$$\mathbf{D} = \begin{bmatrix} E_n^0 & 0 & 0 \\ 0 & E_s^0 & 0 \\ 0 & 0 & E_t^0 \end{bmatrix}, \quad (1)$$

as long as the normal separation Δu_n is less than the critical normal separation Δu_c . Once $\Delta u_n > \Delta u_c$, the spring moduli degrade such that

$$\mathbf{D} = \begin{bmatrix} E_n^0(2 - \frac{\Delta u_n}{\Delta u_c}) & 0 & 0 \\ 0 & E_s(2 - \frac{\Delta u_n}{\Delta u_c}) & 0 \\ 0 & 0 & E_t(2 - \frac{\Delta u_n}{\Delta u_c}) \end{bmatrix} \quad (2)$$

for $\Delta u_c < \Delta u_n \leq 2\Delta u_c$, and vanish for $\Delta u_n > 2\Delta u_c$.

The nonlinear interface constitutive relation is thus

$$\mathbf{f} = \mathbf{D}\Delta \mathbf{u}_{(ns)}, \quad (3)$$

with $\Delta \mathbf{u}$ the relative displacement in local coordinates $(\mathbf{n}, \mathbf{s}, \mathbf{t})$ and \mathbf{f} the conjugate interfacial traction defined on the undeformed reference configuration.

Only failure due to normal separations is accounted for in the current model. While one needs to consider shear failure at an interface for more general situations, it is not difficult to include shear failure into the above interfacial model as demonstrated, for example by Tvergaard and Hutchinson (1993). However, for the type of solid propellant related problems under consideration, the tensile strength of the interface is much lower than the shear strength so that considering the "opening mode" of failure alone encompasses the major damage contribution.

2.2 Stability of an interfacial failure process

In 1992 Suo, Ortiz and Needleman presented a stability analysis for solids possessing interfaces by considering two semi-infinite solids bonded along a plane. Instability of the system was defined as the onset or development of nonunique solutions to the associated boundary-value-problem. In a more global approach Zhong and Knauss (1997a) recently studied the stability of finite solids, with planar or circular interfaces under homogeneous decohesion

(i.e. the whole interface debonds uniformly at the same time) deriving compact stability criteria for a general form of the traction-displacement interfacial relation

$$f = f(\Delta u). \quad (4)$$

For homogeneous decohesion at a bi-material planar interface the stability condition is

$$\frac{2E_{eff}}{L} \geq MAX_{0 < \Delta u < \Delta u_s} \left(-\frac{df}{d\Delta u} \right). \quad (5)$$

where Δu_s corresponds to total separation at the interface. The right hand side of inequality (5) represents the maximum value of $-\frac{df}{d\Delta u}$ when Δu is in $(0, \Delta u_s)$. It is clear that the size of the specimen (L), effective elastic modulus ($E_{eff} = E_1 E_2 / (E_1 + E_2)$), where E_1 and E_2 are the elastic moduli) and the unloading part of the interfacial relation (4) determine the stability of the system. Similar stability conditions are obtained for circular and spherical interface (see Zhong and Knauss (1997a)). For the interfaces in filled elastomers modeled here, E_1 is the modulus of matrix material, E_2 is the modulus of particles, taken here to be infinity because of their relatively high stiffness compared to rubbery binder, so that $E_{eff} = E_1$ (matrix modulus). It is thus clear from the above stability condition (5), that the more compliant the matrix material is, the less stable is the corresponding composite with respect to interfacial failure. Thus particulate-filled elastomers tend to be less stable than particulate metallic composites with respect to the interfacial failure process.

An interfacial failure process associated with inhomogeneous decohesion at interfaces is intuitively more stable than that associated with a homogeneous decohesion. This is so because the surrounding, bonded regions tend to stabilize the decohesion process. Thus the stability conditions obtained by Zhong and Knauss (1997a), though applied only to homogeneous decohesion at interfaces, provide non-conservative estimates for the onset of instability in interfacial failure processes.

The instability due to interfacial decohesion is local because of the rapid (sudden) drop of tractions at the interfaces. This local instability poses a problem for the numerical simulation in a quasi-static setting because it can (and does) lead to the divergence of numerical computations.

3 Formulation of the computational model

We allow for finite deformations and use a three-term Ogden strain energy function for the constitutive description of the matrix as a hyperelastic material. For reference purpose, we summarize here the hyperelasticity theory and its hybrid FEM formulation briefly.

3.1 Hyperelasticity and its FEM formulation

Let Ω_0 be the undeformed reference configuration of the hyperelastic material(s), Ω_t the current deformed configuration, and V_0 and V_t the corresponding volumes. $\mathbf{X} \in \Omega_0$, $\mathbf{y} \in \Omega_t$. If $\mathbf{u}(\mathbf{X})$ is the displacement vector at material point \mathbf{X} , \mathbf{F} the corresponding deformation gradient and J the Jacobian of \mathbf{F} (unit volume change) one has

$$\mathbf{y} = \mathbf{X} + \mathbf{u}(\mathbf{X}), \quad (6)$$

$$\mathbf{F} = \frac{\partial \mathbf{y}}{\partial \mathbf{X}}, \quad (7)$$

$$J = \det(\mathbf{F}). \quad (8)$$

Because the hyperelastic material is (almost) incompressible, the deformation gradient \mathbf{F} is multiplicatively decomposed into its deviatoric and dilatational components, \mathbf{F}^{dev} and \mathbf{F}^{vol} such that

$$\mathbf{F} = \mathbf{F}^{dev} \mathbf{F}^{vol}, \quad (9)$$

$$\mathbf{F}^{dev} = J^{-1/3} \mathbf{F}, \quad (10)$$

$$\mathbf{F}^{vol} = J^{1/3} \mathbf{I}, \quad (11)$$

with \mathbf{I} the identity tensor. It is easy to check that $\det(\mathbf{F}^{dev}) = 1$, $\det(\mathbf{F}^{vol}) = J$ so that \mathbf{F}^{dev} is the volume preserving part of \mathbf{F} , and \mathbf{F}^{vol} its dilatation part.

The strain energy function for a nearly incompressible, hyperelastic solid was given by (Ogden, 1984),

$$W(\mathbf{F}) = \tilde{W}(\mathbf{F}^{dev}) + \phi(J), \quad (12)$$

where \tilde{W} takes account of the deviatoric deformation and ϕ with $\phi(1) = 0$, of dilatational deformations.

Considering frame indifference, and further assuming that the hyperelastic material is isotropic, one has

$$W(\mathbf{F}) = \omega(\tilde{\lambda}_1, \tilde{\lambda}_2, \tilde{\lambda}_3) + \phi(J), \quad (13)$$

where $\tilde{\lambda}_i$ are the principal deviatoric stretches.

Ogden(1972) assumes that ω has the form,

$$\omega(\tilde{\lambda}_1, \tilde{\lambda}_2, \tilde{\lambda}_3) = \sum_{i=1}^N \frac{2\mu_i}{\alpha_i^2} (\tilde{\lambda}_1^{\alpha_i} + \tilde{\lambda}_2^{\alpha_i} + \tilde{\lambda}_3^{\alpha_i} - 3) \quad (14)$$

so that the small strain shear modulus is $\mu_0 = \sum_{i=1}^N \mu_i$ and the relation between the Cauchy stress and the principal stretch is

$$\tau_i = \tilde{\lambda}_i \frac{\partial W}{\partial \tilde{\lambda}_i} - \left(\frac{1}{3} \sum_{i=1}^N \tilde{\lambda}_i \frac{\partial W}{\partial \tilde{\lambda}_i} - J \frac{\partial \phi(J)}{\partial J} \right). \quad (15)$$

If the material is incompressible ($J = 1$), one has $\phi(J) = 0$, and the corresponding stress-stretch relation is

$$\tau_i = \lambda_i \frac{\partial W}{\partial \lambda_i} - P_i \quad (16)$$

where P_i is an arbitrary pressure and λ_i are the principal stretches.

For nearly incompressible material, the usual displacement finite element formulation can "behave poorly" because the effective bulk modulus is very large compared to its shear modulus, which cause the stiffness matrix to be almost singular from a numerical point of view. Consequently, the stress calculated at the numerical integration points show large oscillation in the pressure. To avoid this, a hybrid element or mixed formulation has been proposed (see for example, Simo and Taylor(1991)).

3.2 Interface element

The interfacial constitutive relation is implemented by constructing an interface element by the principle of virtual work (Beer (1985)) by the following steps: (1) Set-up local coordinates (\mathbf{n} , \mathbf{s} , \mathbf{t}) to describe the interface geometrically; (2) Find the relative displacements at the interface in local coordinates; (3) Use the principle of virtual work and the interfacial constitutive relation to obtain an equilibrium condition for the interface element in terms of

global nodal coordinates. One then assembles the interface element stiffness matrix with the remaining element stiffness matrices to form the global stiffness matrix.

If F^e is the force vector for nodes of the interface element, a is the element displacement vector and \mathbf{B} the transformation matrix between nodal displacements and displacement in the local coordinates. Then, with point (3) in mind one has

$$\int_{interface} \mathbf{B}^T \mathbf{f} ds = F^e, \quad (17)$$

or

$$\int_{interface} \mathbf{B}^T D B a ds = F^e, \quad (18)$$

If n refers to time steps, k refers to the sequence of iterations, the residual force due to the interface element is

$$R = - \int_{interface} B^T D_n^{(k)} B ds a_n^k \quad (19)$$

and the tangent stiffness matrix of the interface element becomes

$$\mathbf{K}_t = - \frac{\partial R}{\partial \mathbf{u}}. \quad (20)$$

For the interfacial relation (3), the tangent stiffness matrix for interface elements is non-symmetric. Using the tangent stiffness matrix may be a source of numerical difficulty since the stiffness matrix for the bulk material is symmetric. We use direct iteration, which is expressed for the interface elements by

$$\int_{interface} B^T D_n^k B ds \{\Delta a\} = F_n^{(k+1)e} - \int_{interface} B^T D_n^k B ds \{a_n^k\} \quad (21)$$

where $a_n^{(k+1)} = a_n^k + \Delta a$. The implementation of the FEM formulation for hyperelasticity is available in ABAQUS 5.5, and the interface element (interfacial constitutive model; the element has initially zero thickness) is incorporated into that code by way of a user subroutine.

4 Numerical results

We consider plane strain deformation in the modeled two-dimensional composites. The matrix characteristics are determined by fitting the parameters in the 3-term Ogden function

to the experimental data of Treloar(1940). The parameters are $\mu_1 = 58.23MPa$, $\alpha_1 = 1.029$, $\mu_2 = 1.35 \times 10^{-5}MPa$, $\alpha_2 = 10.707$, $\mu_3 = 0.246MPa$, $\alpha_3 = -2.957$; these satisfy the material stability condition. The parameters in the interfacial element are chosen such that the maximum f_n at an interface is of the same magnitude as that observed in relevant uniaxial tensile experiments (Vratsanos and Farris(1993)). The specific parameter values chosen are $E_n = 10^3MPa$, $E_t = 10^4MPa$ and $\Delta u_c = 10^{-5}m$.

The numerical integration of the interface element stiffness matrix is carried out by a 2-point Gaussian quadrature. Due to the inherent proclivity towards instability of the debonding process, all the numerical examples are examined under displacement controll. As a convention, we mean the Cauchy stress when writing "stress" unless specified differently and the word "strain" connotes nominal strain.

The common approach to analyze properties of composites, whether by numerical or closed form methods involves the "unit cell" approach. It is implicit in this approach that (a) filler particle sizes are "distributed" uniformly and periodically and (b) the unit cell characteristics are adequately indicative of global response of the composite. With the intent of questioning the latter assumption we examine thus particle size variations and divide the effort arbitrarily into consideration of small and large variations in particle size.

4.1 Interaction of inclusions: small variations in inclusion sizes

Three cases are considered: composites with low volume fraction (8.7%), intermediate volume fraction (35.0%) and high volume fraction (68.4%) of particles³. In these three cases we analyze a square domain containing 4-inclusions with different radii. For reference purpose, we also analyzed the counterparts of these problems with identical inclusions, the radii of which are the mean of the inclusion radii for the non-uniform configuration. In the sequel we refer to the geometry with identical particle size as case 1 and to the situation with different particle size as case 2. The radii of inclusions and their mean values for each case are listed in table 1; where we associate the case number 1, 2, 3 with volume fractions; particle size variations are sub-cases as in 1.1 and 1.2 for example for case 1.

³The upper limit of volume fraction is 78.5%, for uniformly distributed "rods" in a (two-dimensional) composite and 52.4% for uniformly distributed spherical particles

Table 1: Inclusion radii and mean radii

Case	Inclusion1 radius	Inclusion2 radius	Inclusion3 radius	Inclusion4 radius	Mean radius	volume fraction
1	0.49	0.51	0.52	0.48	0.5	8.7%
2	1.1	1.0	0.99	1.05	1.035	35.0%
3	1.41	1.42	1.39	1.38	1.4	68.4%

The boundary conditions are imposed according to Figure 2: Two opposing sides of a square elastomer are displaced uniformly in opposite directions by a prescribed amount and the remaining, latera surfaces remain traction free. for the case of uniform inclusions, we take advantages of symmetry conditions.

Low volume fraction of inclusions (case 1)

Comparing stress distribution for case 1.1 (inclusions with same radius) and case 1.2 (inclusions with differnt radii) at several global strain stages (roughly 5%, 10% and 16%), there is no significant difference between the two subcases. This observation is further supported by the little difference between global stress strain response of these two subcases. (As the volume fraction is low, the difference between the particulate composites and the pure elastomer is small, too). These results were reported earlier by Zhong and Knauss (1997b).

These observations indicate that when the volume fraction of inclusions of a composite is small, the interaction between particles is weak, and thus unit-cell approach or damage-incorporating constitutive model can be applied with confidence even though the sizes of fillers vary a little.

Intermediate volume fraction of inclusions (case 2)

Case 2.1: Inclusions with same radius

We observe that 1) the vacuoles formed at the interfaces between the matrix and the four inclusions are the same (obvious due to the symmetry condition); 2) the size of cavities formed at the interfaces increase as the applied strain increases from 1.2% to 5%, as expected.

Case 2.2: Inclusion with different radii

From stress contours one observes several features⁴: 1) cavities formed at the interfaces between the matrix and the four inclusions are not the same; 2) interfacial failure process at the interfaces are significantly different between case 2.1 and case 2.2: in case 2.1, voids formed at interfaces will grow monotonically, in case 2.2 voids formed at interfaces can grow as well as shrink due to inclusion interactions. The second observation is supported also by the difference in the global stress strain responses for the two subcases, as shown in Figure 3. In Figure 3, we see clearly that the stress strain curves for the two subcases are essentially the same when global strain is smaller than 2.5%. However, when this strain exceeds 2.5%, kinks in these two stress strain curves occur at different strain levels and their profiles have distinct features. (Kinks in stress strain curves indicate substantial debonding at interfaces).

So when the volume fraction of inclusions is at intermediate level, interactions between inclusions are moderate, but effects of these interactions on the damage evolution are easily identifiable from global stress strain curve.

High volume fraction of inclusions (case 3)

When the volume fraction is as high as 68.4%, one observed pronounced effects of particle interaction and of variation of particle sizes.

Case 3.1: Inclusion with same radius

We report the stress contours in Figures 4a, 5a, we see that (1) debonding occurs at interfaces near symmetry plane perpendicular to the direction of loading, (2) separations grow with the increase of global strain, (3) when the global strain is around 10%, the interface cavities look similar to those predicted by unit cell analyses.

Case 3.2: Inclusions with different radii

When the sizes of the 4 inclusions are slightly different, it is observed (Figure 4b, 5b) that (1) debonding occurs at the larger inclusions first, (2) cavities formed at interfaces grow or shrink with the increasing global strain (this is impossible in a unit cell analysis). This second observation is clearly a strong indication of the significant effect of the interactions between particles and also of the significant effect of even a slight variation in particle sizes.

The interaction of particles and variation of inclusion sizes jointly control the damage

⁴To save space, we do not display stress contours here. More detailed numerical results are given for case 3 where significant effects of size variation are observed

evolution process as well as the global material response. The global stress strain curves shown in Figure 6 indicates that when significant debonding occurs (indicated by the kink at 0.2% global strain), the material responses differ substantially between a composite with the same size of inclusions and a composite possessing inclusions of different sizes.

A 16-inclusion problems (case 4)

A square with 16 inclusions was also considered for which the inclusion sizes fluctuate around a mean of 0.4 rendering a volume fraction of 50%. Again, normal displacements are described at two opposite sides of the domain with the remaining two sides being traction free. For this case the computation reaches 4% global strain with the largest normal strain in the interior being 23%; thereafter the algorithm diverges.

A detailed examination of the results for this case shows that (1) interaction between particles control the damage evolution process; (2) a small change in particles sizes has a significant effect on damage evolution and material response (see Figure 6ab in Zhong and Knauss (1997b)). In addition, discrete segmental increases are observed in the global stress-strain curve.

The 4 cases considered here indicate that the interaction of particles and even the slight variation in the particle size control damage evolution in a "particulate" composite and its local stress strain response.

4.2 Interaction of inclusions: large variation in inclusion size

Again we consider a square domain with 16 inclusions with different radii as indicated in Figure 7 (considering symmetry, only a quarter of the domain is displayed). The particle sizes are arranged as shown on purpose so that one can take advantage of the symmetry conditions involved.

From Figures 8 - 9, we observe that (1) debonding occurs at interfaces between the largest particle and matrix first, and subsequently at interfaces of smaller particles (of descending size) and matrix; (2) there is essentially no debonding at the interfaces between the smallest particles (about half the size of the large particle) and the matrix even when the global strain is 8% or so.

Again, we observed that the interaction between particles plays important role in the

damage (debonding) evolution process. It seems that a bimodal distribution of particles in an elastomer produce some distinct features of damage evolution and material response (See Figure 10, and also compare Figure 10 with Figure 7 and Figure 6a of Zhong and Knauss (1997b))

The strong effect of interaction between particles and the significant effect of the slight variation of particle sizes (for high volume fraction of particles) cannot be predicted by unit cell analyses or damage-incorporating constitutive models. These effects might contribute to failure mechanisms in particulate composites with high volume fraction of particles such as solid propellants (volume fraction 70 - 90 %). Nakamura et. al. (1992) investigated experimentally the effect of the particle size on the fracture toughness of epoxy resin filled with spherical silica. They found that both critical stress intensity factor and critical energy release rate increased with (mean) particle size. This can be easily explained by the fact that when the (mean) particle size is large, significant damage (in the form of interfacial debonding) occurs at a crack tip. This damage zone can consume stored strain energy at the crack tip and thus hamper crack propagation. Our results seem to be in line with their observations and support the above explanation in the following way: The proposed model predicted that the larger the particle size is, the easier is the debonding. The interfacial failure process consumes part of the strain energy. This correlation between numerical and experimental observations is indirect because we did not consider the effect of interfacial failure on fracture toughness in our numerical study yet. In addition, our results also suggested that the standard deviation of particle size distribution should have significant effect on fracture toughness. Comparing global stress strain response of composite of same size inclusions and that of composite with inclusions of slightly different size, the interfacial failure process in the latter composite consumed more energy than that in the first composite. We expect that the fracture toughness for the latter composite (small variation in inclusion sizes) will be larger.

5 Conclusions

By characterizing the particles, matrix and interfaces in a particulate-filled elastomer individually, the whole failure process (interfacial debonding, growth of voids formed at interfaces) is analyzed by the FEM.

It is shown that (1) When the volume fraction is high, even small changes in particle size can have a large effect on local material response and on damage evolution in particular; (2) When there is a large difference in particle sizes (such as bimodal distribution), separation damage occurs at interfaces between the large particles and matrix, little or no damage occurs at small ones. It seems that bimodal distribution of particles in an elastomer produce some distinct features of damage evolution and local material response.

Although the effects of inclusion size (small) variation on local material response may be smoothed out for an ensemble with large number of inclusions, it seems likely that the change in local material response will affect failure process (e.g. interfacial debonding) as well as continuum material properties such as fracture toughness.

In order to analyze the interaction of particles with a macroscopic crack, such as propagation of a macroscopic crack via the growth and coalescence of voids, the computational approach must be made more robust and stable. This type of investigation may lead to a better understanding of failure mechanism in filled elastomers.

Acknowledgment

The work reported here has been supported by Air Force Office of Scientific Research under grant F9620-94-1-0253, with Major B. Sanders and Dr. O. Ochoa as monitors. We benefited from discussions with Dr. C. T. Liu of Phillips Laboratory, Edwards Air Force Base. We are grateful to Hibbitt, Karlsson & Sorensen, Inc. for making the ABAQUS finite element code available to us under an academic license. We are also grateful to NSF/UCSD San Diego Supercomputer Center where part of the computations were carried out.

References

- [1] Beer, G. (1985), An isoparametric joint/interface element for finite element analysis, *Int. J. Num. Methods Eng.*, 21, 585-600.
- [2] Farris, R. J. and Schapery, R. A. (1973), Development of a solid rocket propellant nonlinear viscoelastic theory, Technical Report AFRPL-TR-73-50 , Air Force Rocket Propulsion Laboratory, Edwards, CA.
- [3] Govindjee, S. and Simo, J. C. (1992), Transition from micromechanics to computationally efficient phenomenology: carbon filled rubbers incorporating Mullins effect, , *J. Mech. Phys. Solids*, 40, 213-233.
- [4] Nakamura, Y. , Yamaguchi, M. , Okubo, M. and Matsumoto, T. (1992), Effect of particle size on the fracture-toughness of epoxy-resin filled with spherical silica, *Polymer*, 33(16), 3415-34-26.
- [5] Needleman, A. (1987), A continuum model for void nucleation by inclusion debonding, *ASME J. App. Mech.*, 54, 525-531.
- [6] Ogden, R. W. (1972), Large deformation isotropic elasticity: on the correlation of theory and experiment for incompressible rubber like solids, *Proc. R. Soc. Lond. A*, 326, 565-584.
- [7] Ogden, R. W. (1984), Non-linear elastic deformation, Ellis Horwood Limited.
- [8] Ravichandran, G. and Liu, C. T. (1995), Modeling constitutive behavior of particulate composites undergoing damage, *Int. J. Solids Structures*, 32(6/7), 979-990.
- [9] Schapery, R. A. (1986), A micromechanical model for nonlinear viscoelastic behavior of particle-reinforced rubber with distributed damage, *Eng. Fract. Mech.*, 25, 845-867.
- [10] Simo, J. C. and Taylor, R. L. (1991), Quasi-incompressible finite elasticity in principle stretches: continuum basis and numerical algorithms, *Computer Methods in App. Mech. and Eng.*, 85, 273-310.

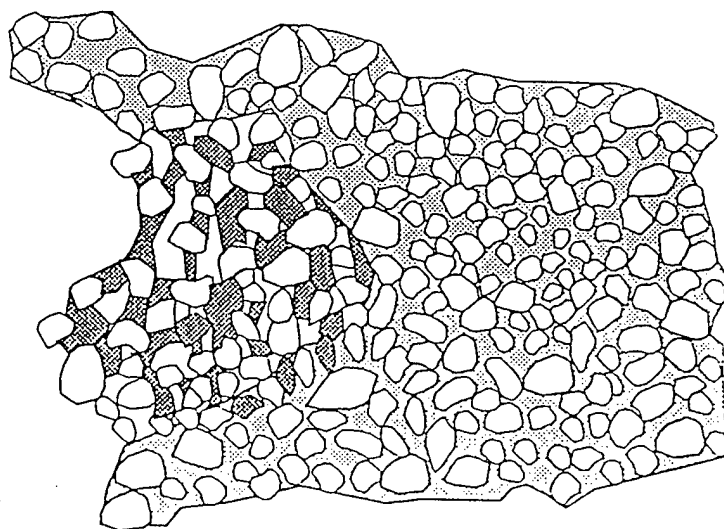
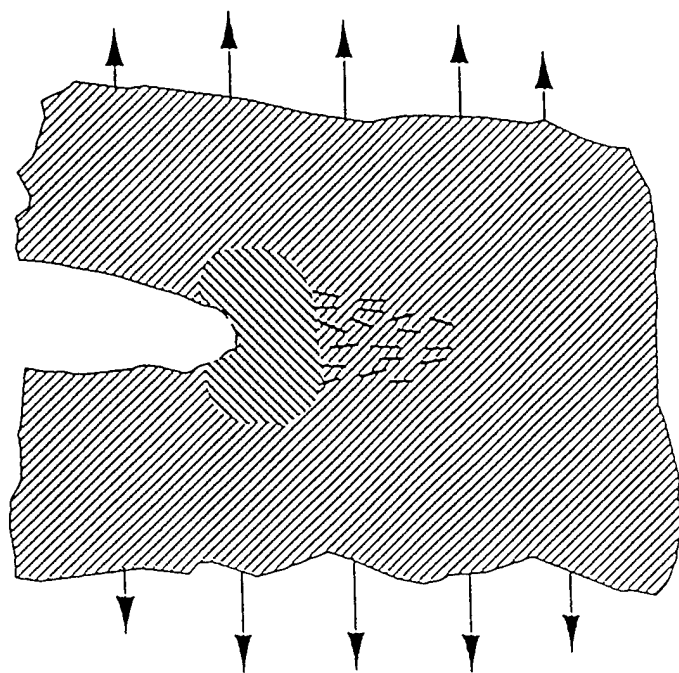


Figure 1. A discretely failing region embedded
in a linear/nonlinear material

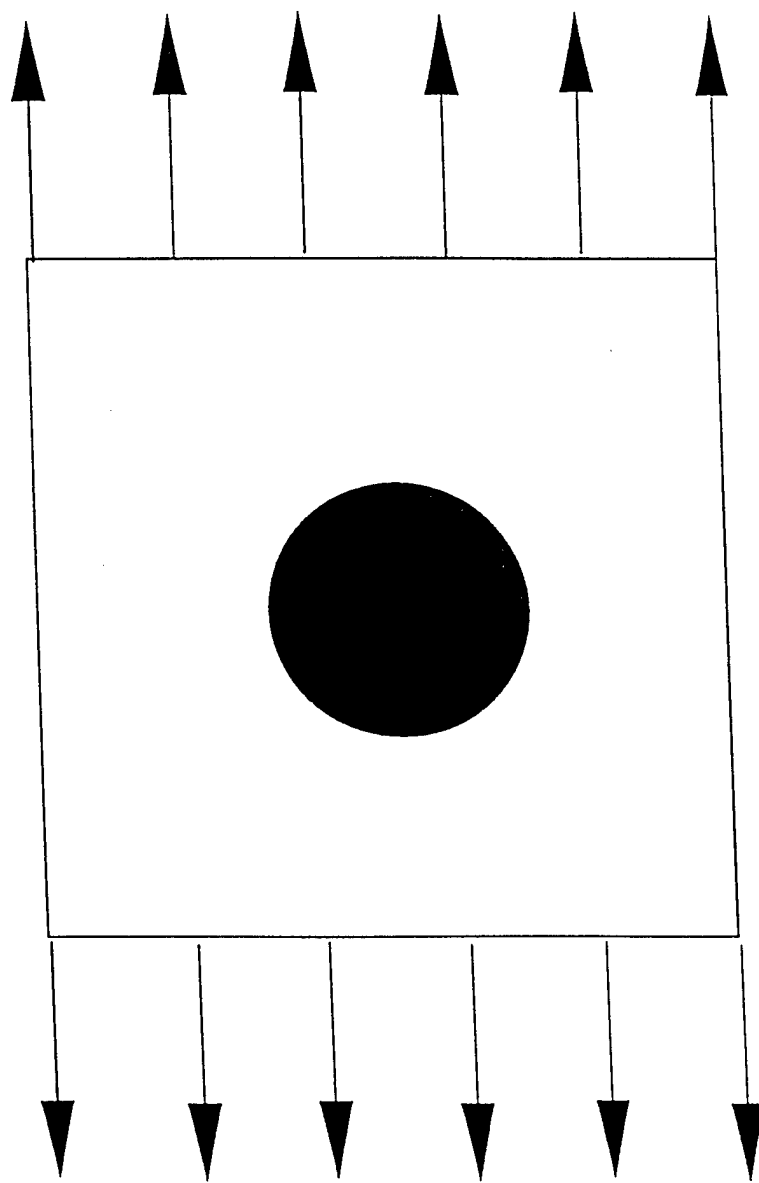


Figure 2: Boundary conditions prescribed in the computations

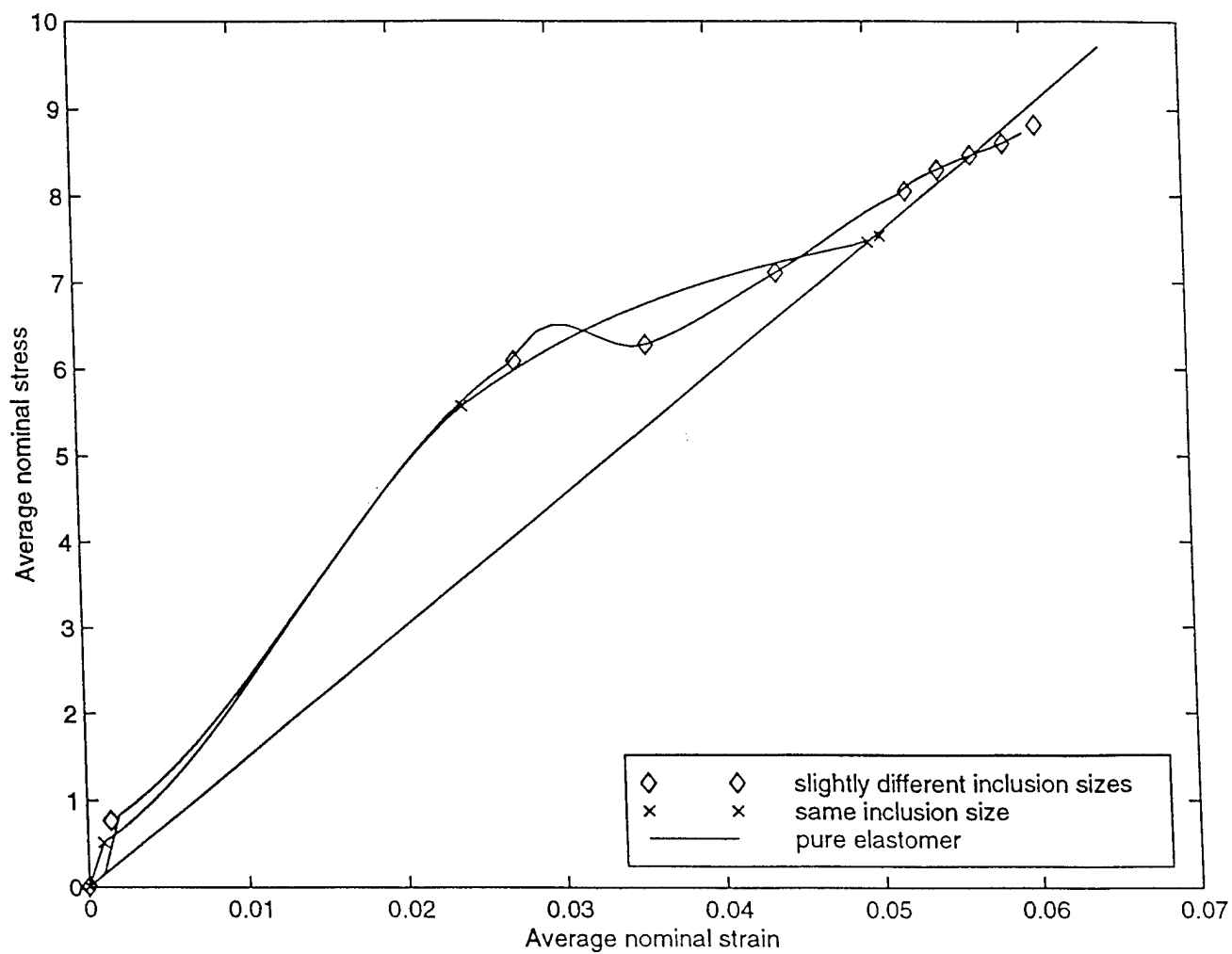
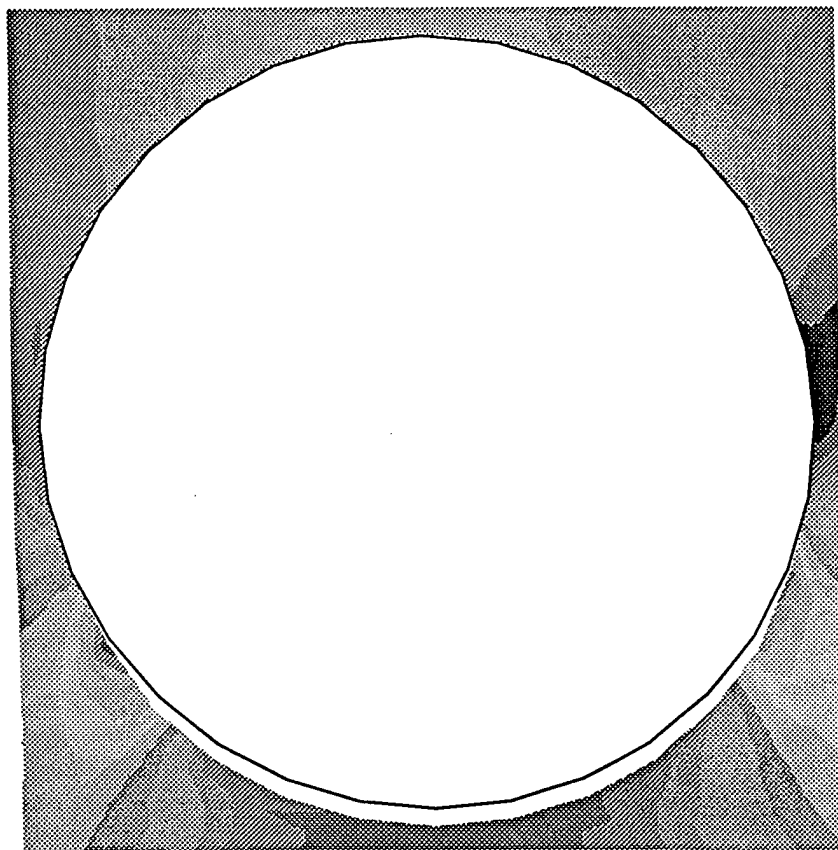
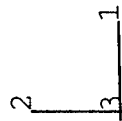
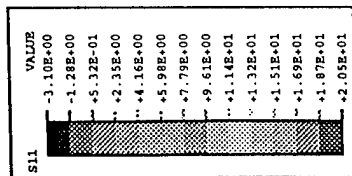


Figure 3: Average nominal stress strain curves for intermediate inclusion volume fraction.



line of symmetry

Figure 4a: Contour of S11 for large volume fraction: identical inclusions (only a quarter of the sample is shown, 2.0% global strain)

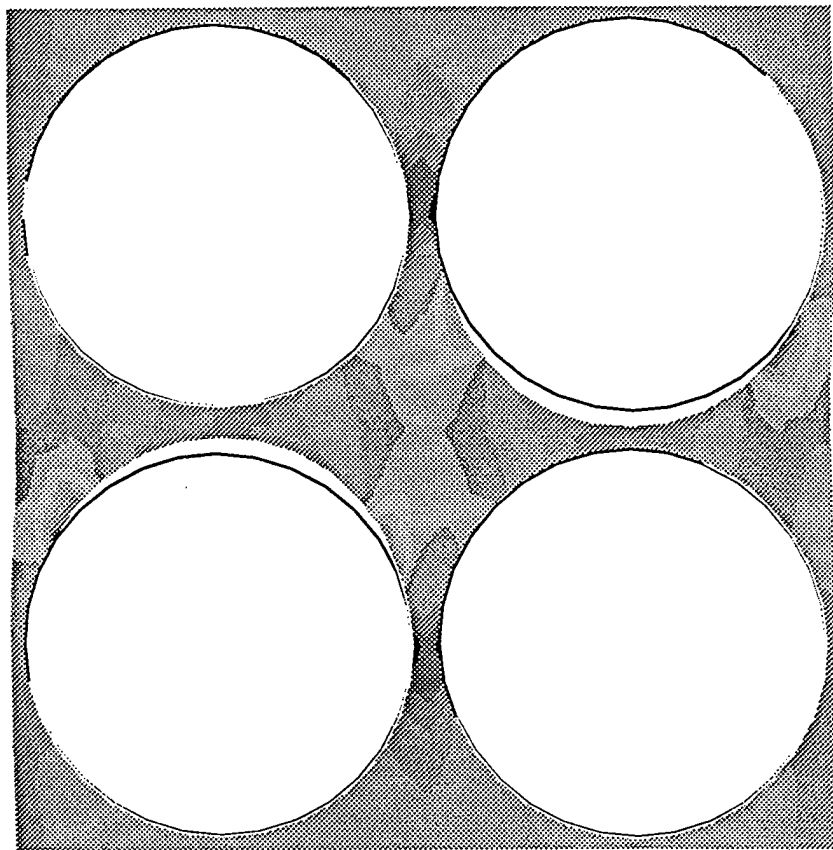
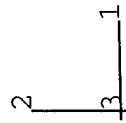
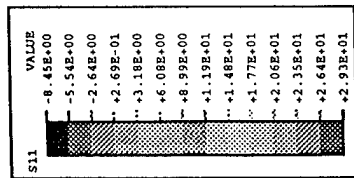


Figure 4b: Contour of S11 for large volume fraction case: different inclusion sizes (2.0% global strain).

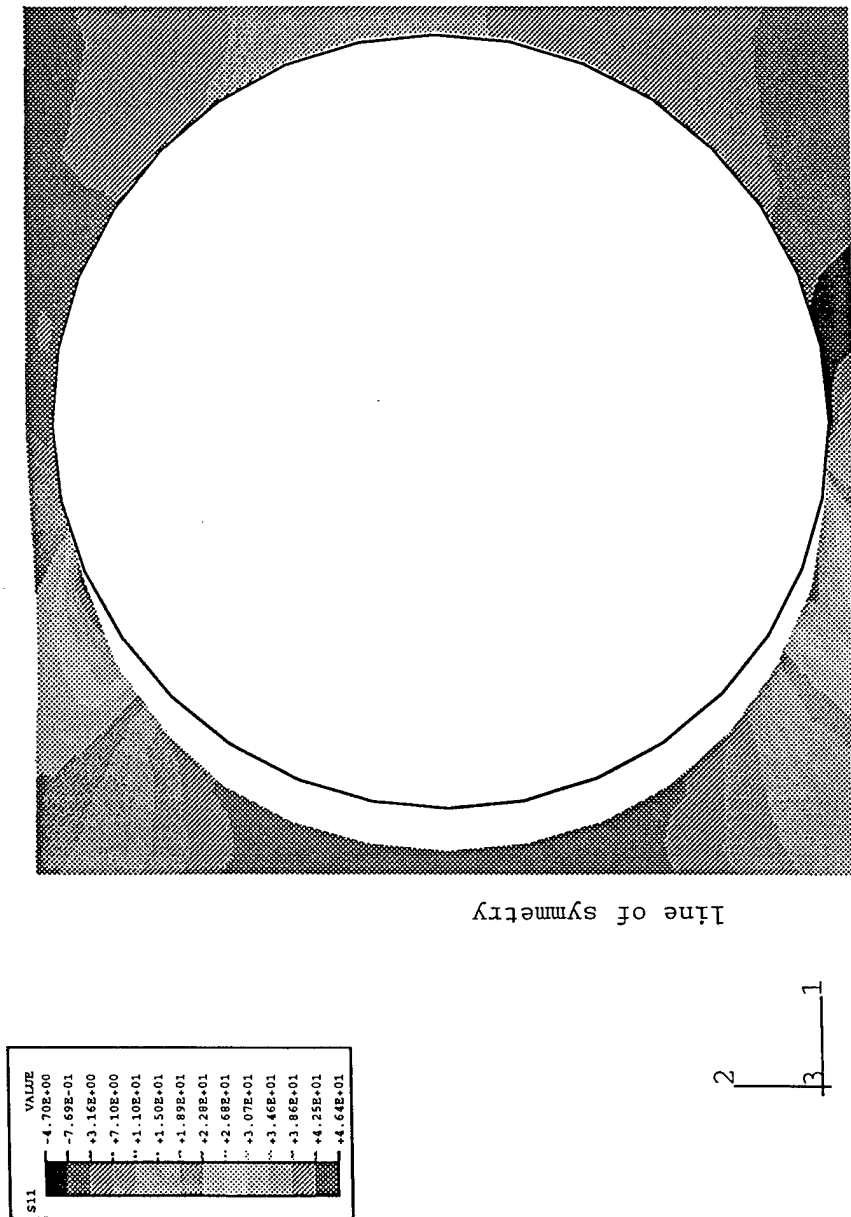


Figure 5a: Contour of S11 for large volume fraction: identical inclusions (only a quarter of the sample is shown, 5.4% global strain).

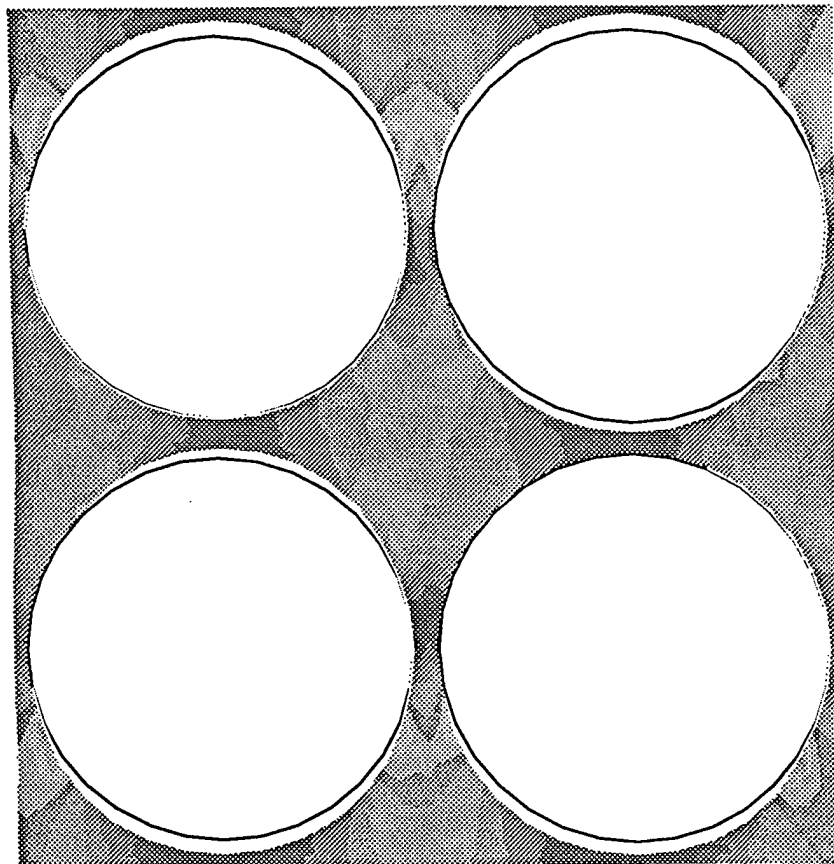
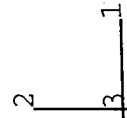
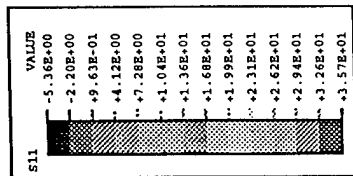


Figure 5b: Contour of S11 for large volume fraction case: different inclusion sizes (4.3% global strain).

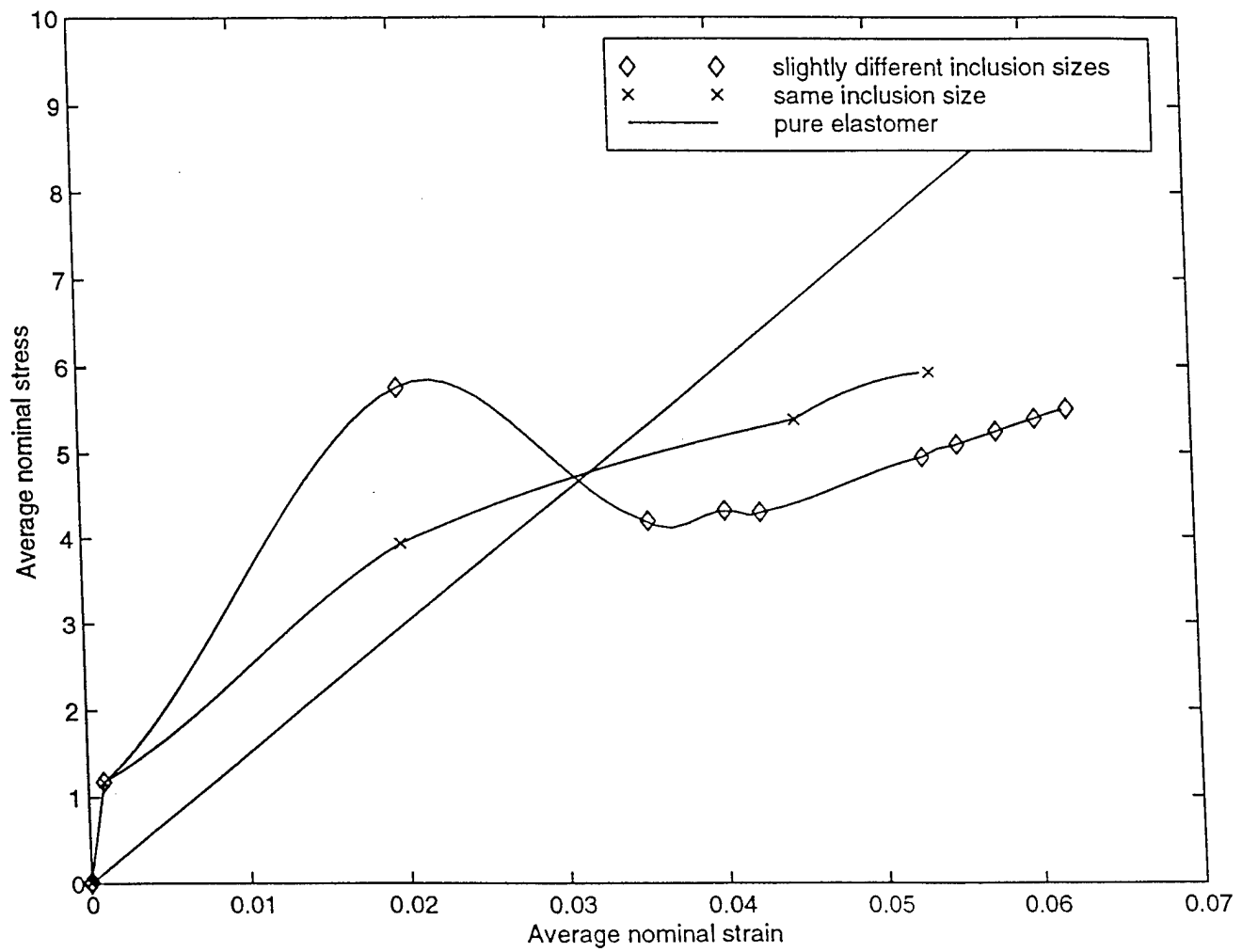


Figure 6: Average nominal stress strain curves for large volume fraction cases.

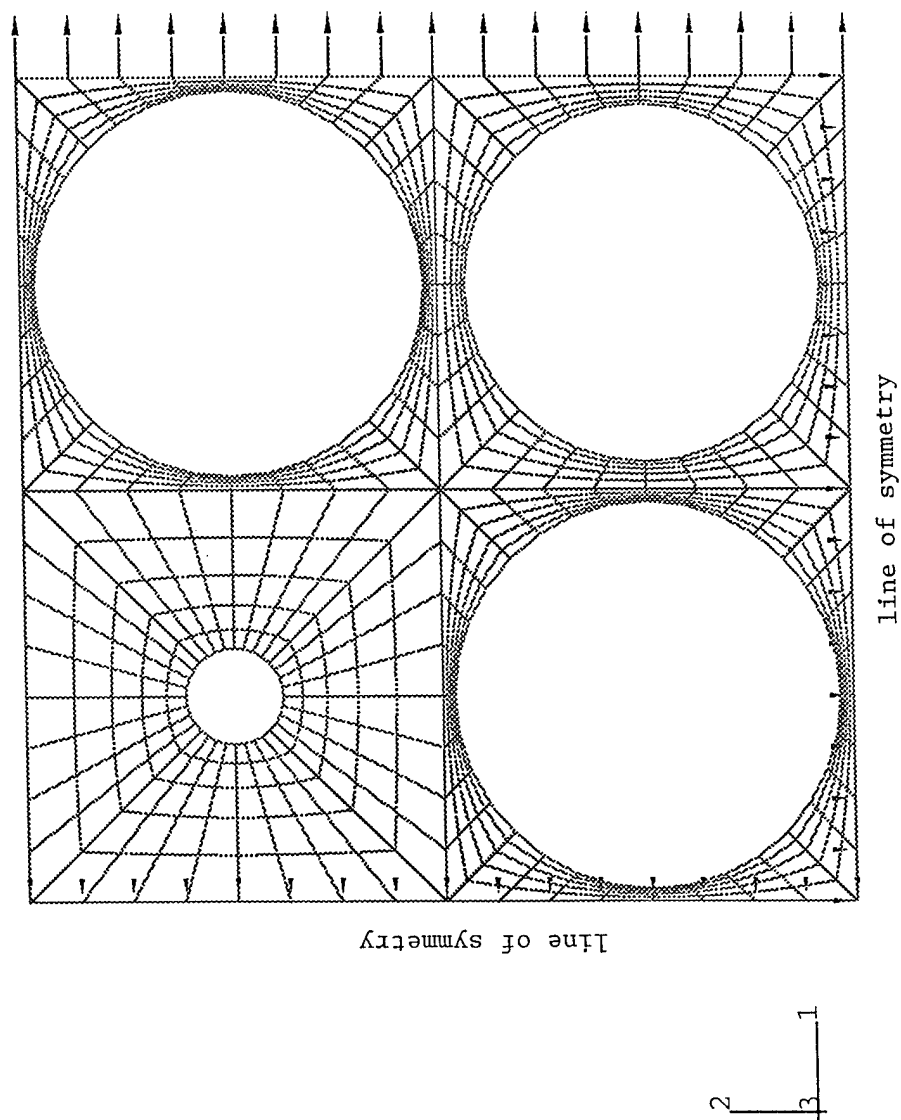


Figure 7: Bimodal size distribution of inclusions (only a quarter of the sample is shown here).

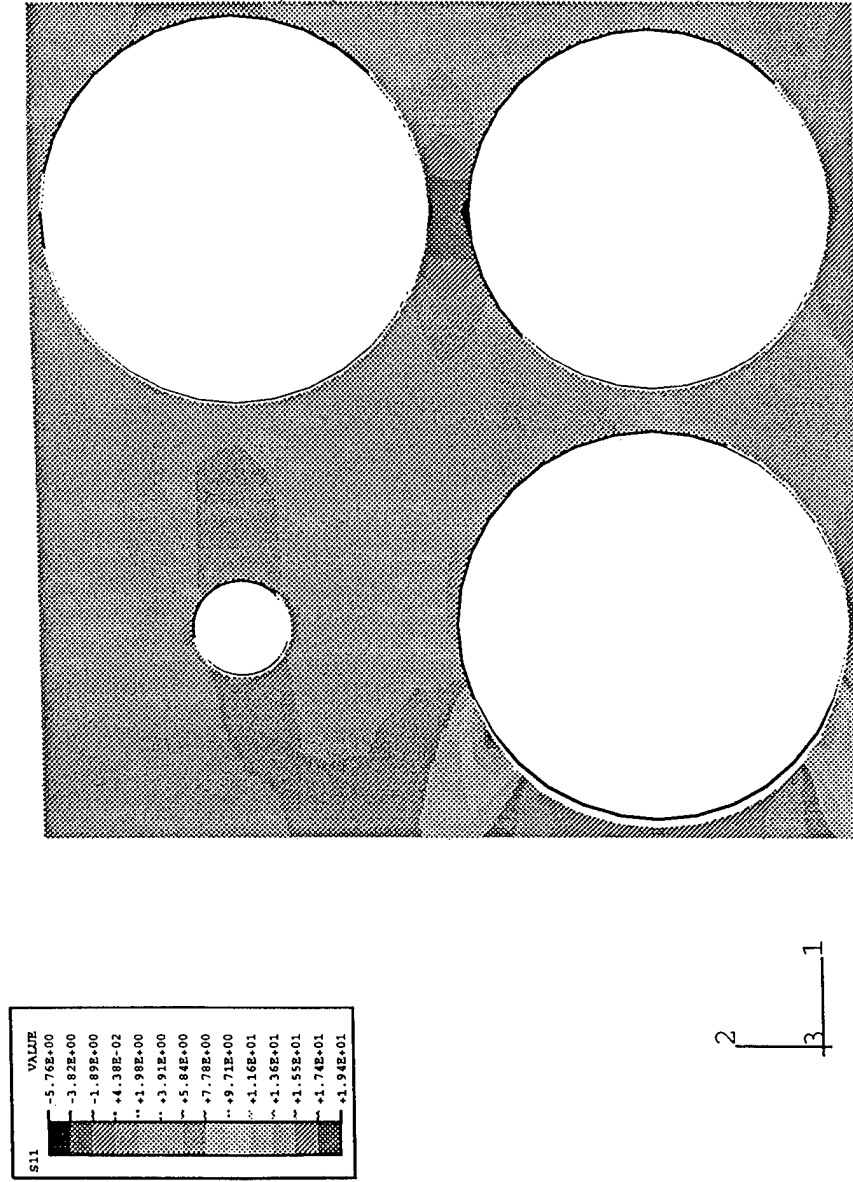
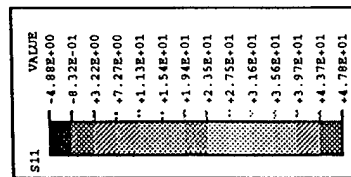


Figure 8: Contour of S11 for bimodal size distribution case (2.2% global strain).



2 1 3

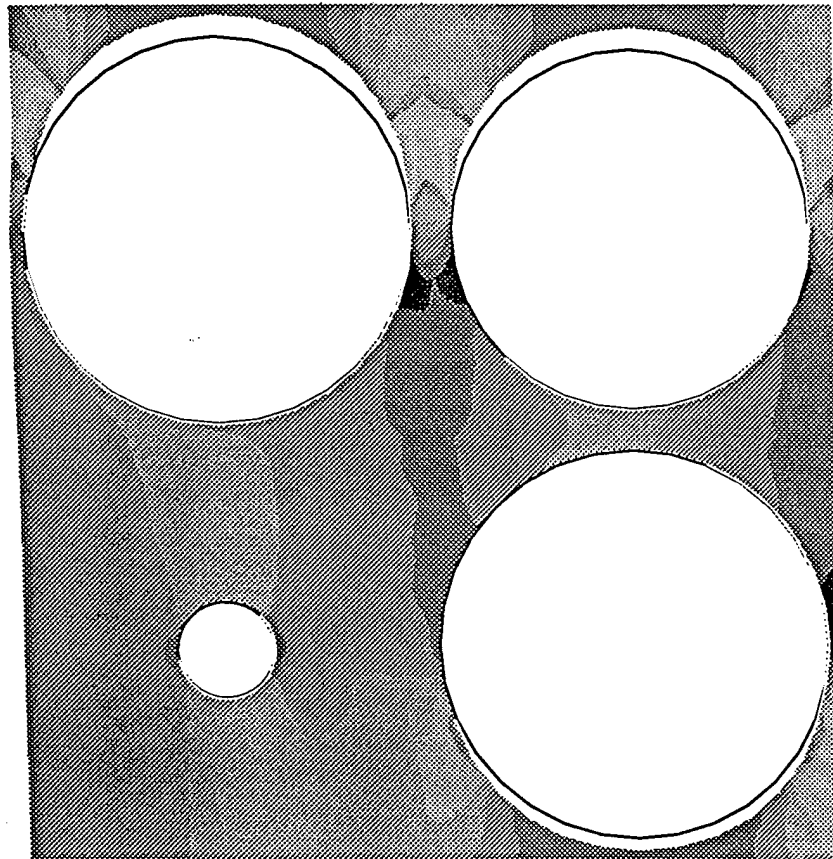


Figure 9: Contour of S11 for bimodal size distribution case (7.5% global strain).

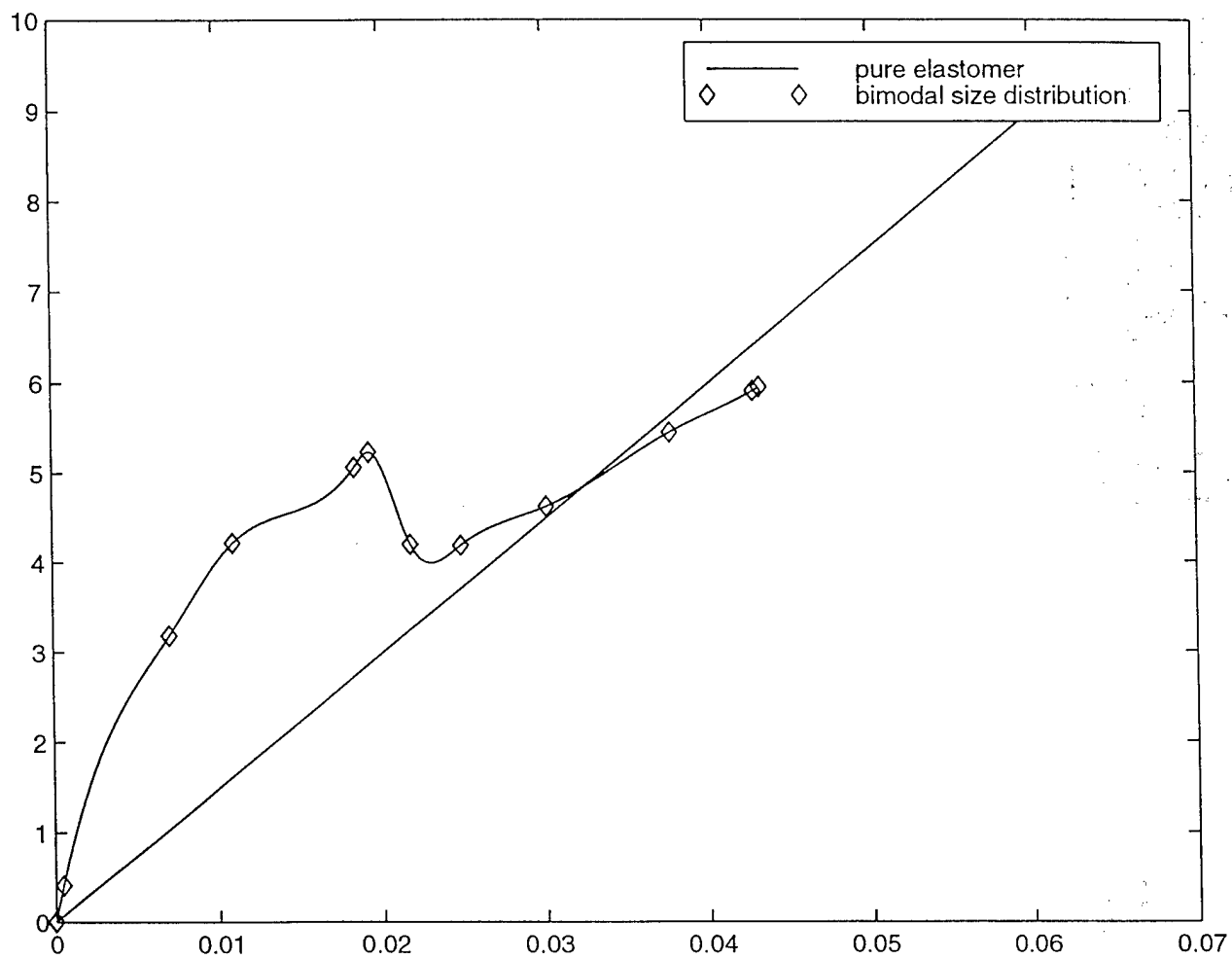


Figure 10: Averagare stress strain curve for bimodal size distribution case.